Omega-P, Inc.
199 Whitney Avenue, Suite 200
New Haven, CT 06511

Final Report to Department of Energy
SBIR Grant DE-FG02-03 ER 83736

QUASI-OPTICAL 34-GHz PULSE COMPRESSOR

TABLE OF CONTENTS

Work on this project was carried out by A.L. Vikharev, A.M. Gorbachev, O.A. Ivanov, V.A. Isaev, S.V. Kuzikov, V.A. Koldavov; with J. L. Hirshfield serving as Principal Investigator. This report was written by Dr. Vikharev and Dr. Hirshfield

June 15, 2007

I. INTRODUCTION

Omega-P, Inc. proposed and was awarded a Phase I and Phase II Grants DE-FG02-03-ER83736 to design and test quasi-optical passive and active* RF pulse compressors to operate at 34.272 GHz. The objective of the project was to demonstrate that this new millimeter (mm)-wave technology will be suitable for compressing RF pulses from a high-power mm-wave magnicon, thereby increasing peak power levels to the 100's of MW level for studying mechanisms that limit the magnitudes of RF electric and magnetic fields that can be sustained near material surfaces and, eventually, for perhaps driving a high-gradient accelerating structure. The proposed work was a continuation of that initiated under a 2001 DoE SBIR Phase I grant DE-FG02-01-ER83238. The chosen frequency was 34.272 GHz, three times the NLC frequency 11.424 GHz, which at the time seemed a natural choice in an upgrade scenario to extend the X-band NLC center-of-mass energy from 0.5 up to at least 2.0 TeV. That scenario has been rendered moot by the decision in August 2004, that the technology of choice for ILC is superconducting RF, with linac operation at a frequency of 1.3 GHz and with an acceleration gradient of 31.4 MeV/m. But the importance of 34-GHz high-power technology as a tool for basic studies aimed towards achievement of high-gradients (>100 MeV/m) in warm (non-superconducting) structures has not been diminished. It is to strengthen that technology that the present project is directed.

Omega-P has pursued several interrelated R&D projects on topics aimed at development of a high-gradient electron test facilities at 34.272 GHz that could lead to acceleration structures for a future high energy collider. These topics include development of a 45-MW pulsed magnicon, of a high-gradient accelerator structure, of ancillary high-power rf components for distributing power from the magnicon to accelerator sections, of a resonant ring for producing circulating power levels near the GW level for component testing, and of a quasi-optical RF pulse compressor to produce the high peak power RF pulses for driving the accelerator module (the project discussed here). Studies at 34 GHz are also underway of surface fatigue due to intense pulsed temperature excursions. The key element in all this high-gradient R&D is the Omega-P/Yale 34-GHz, 45-MW, magnicon [1] onto which output windows and transmission lines have recently been installed, prior to initiating experiments using its output power. Production of the intense RF peak powers (100's of MW) contemplated for driving a mm-wave accelerator module will require an efficient RF pulse compressor that can transform an output pulse of given peak power and pulse width from the magnicon into a pulse of higher peak power and shorter width. At millimeter (mm) wavelengths, with required peak powers of 100's of MW, open (so-called "quasi-optical") RF structures are required so that the pulse compressor elements can withstand high RF fields without breakdown. The project described here has as its goal the design, fabrication, and demonstration of prototypes of passive and active quasi-optical 34-GHz pulse compressors for use in testing candidate high-gradient accelerator structures.

Motivation for developing high-power mm-wave technology, including an RF source, accelerating structure, associated components, and an RF pulse compressor, is provided by the assumed classical scaling of accelerating gradient with frequency, which is approximately linear [2]. Thus NLC, operating at 11.424 GHz, was to achieve an unloaded accelerating gradient of 77 MV/m [3], approximately four times greater than that achieved at 2.856 GHz at SLC. The same scaling suggests that at 34.272 GHz the unloaded acceleration gradient could exceed 200 MV/m.

*RF pulse compressors are customarily defined as being either *active* or *passive* if their rf circuit properties are *altered* (i.e., switched), or *stationary*, during the applied RF pulse.

So one compelling reason for a coordinated mm-wave (Ka-band) technology development program is to establish (or not) this anticipated scaling with firm laboratory evidence; and of course to demonstrate the high acceleration gradient. Further, laboratory tests would allow confirmation (or not) of the widely accepted scaling with frequency of field emission and RF breakdown in high-gradient room-temperature linac structures, as elucidated by Wang and Loew [4]. Tests have been performed with μs-length pulses at S, C and X-band; and at 30 GHz with 12 ns pulses on the CLIC structure [5]. But extension upwards in power and pulse length are required to further probe the scaling laws at 34.272 GHz in a regime where a possible future high-gradient linac would operate, namely with RF surface electric field gradients greater than 0.5 GV/m and pulse widths of about 100 nsec. The RF pulse compressors developed as described here are necessary for carrying out these studies in a test facility being established in the Yale Beam Physics Laboratory for R&D on mm-wave high-gradient accelerator technology.

In the context of this report it is also important to mention that strong interest was expressed by the CLIC group at CERN for entering into collaboration with Omega-P with the objective of employing power from the Omega-P 34-GHz magnicon to evaluate CLIC structures. For such tests the CLIC structures would be scaled from 30 to 34 GHz. However, since the CLIC Study Group has recently reduced its operating frequency to 12 GHz, interest in conducting tests at 34 GHz has waned somewhat, but not entirely vanished.

II. STATUS OF MAGNICON TEST FACILITY

A necessary step towards evaluating the quasi-optical Ka-band pulse compressor is the establishement of the Ka-band test facility powered by the Yale/Omega-P 45-MW, 34-GHz magnicon amplifier that is designed to operate with a 1.5 μs pulse length [1]. This tube was built with support under DoE SBIR Phase II grant DE-FG02-97-ER82446. Photographs of the 34-GHz magnicon installed in the Yale Beam Physics Laboratory are shown in Fig. 1. The blue assembly dominating the pictures is a cylindrical stack of lead bricks for x-ray shielding. The 500 kV pulse transformer and 0.62 μP electron gun are installed in the oil-filled tank at the bottom. WR-90 rf input and sampling waveguides and WR-28 output waveguides all exit the tube below an iron yoke surrounding the cryomagnet that provides the non-uniform magnetic field (up to 2.3 T) required for beam transport and resonant interaction between the beam and the seven cavities of the magnicon. (This magnicon is a frequency-tripler, with output frequency three times the input frequency.) The four WR-28 outputs of the tube are connected through high-power directional couplers and step-motor driven phase shifters to 63-mm output windows and transmission lines. In the photographs of Fig. 1, the transmission lines terminate in vacuum loads for RF conditioning of the transmission lines and for calorimetric power measurements. Eight forward and reverse signals from the WR-28 couplers, and five signals in WR-90 waveguide or low-loss coax are brought into the experimental control area, where instrumentation includes the 11.4 GHz input drive chain, monitoring gauges for 23 ion pumps on the tube and transmission lines, three power supply controllers for the cryomagnet coils, and detectors for the 13 microwave and millimeter-wave signals. In addition, a WR-28 slotted line and X-band precision wavemeter are used for measuring frequency and confirming that the output from the tube is monochromatic. All signals are digitized for storage, manipulation, display, and plotting. The third photograph in Fig. 1 shows the 1-m diameter tank into which the passive and active quasi-optical RF pulse compressors are to be installed for high-power tests using, at first, output from one of the transmission lines. Experiments are scheduled to commence in late-Summer 2007.

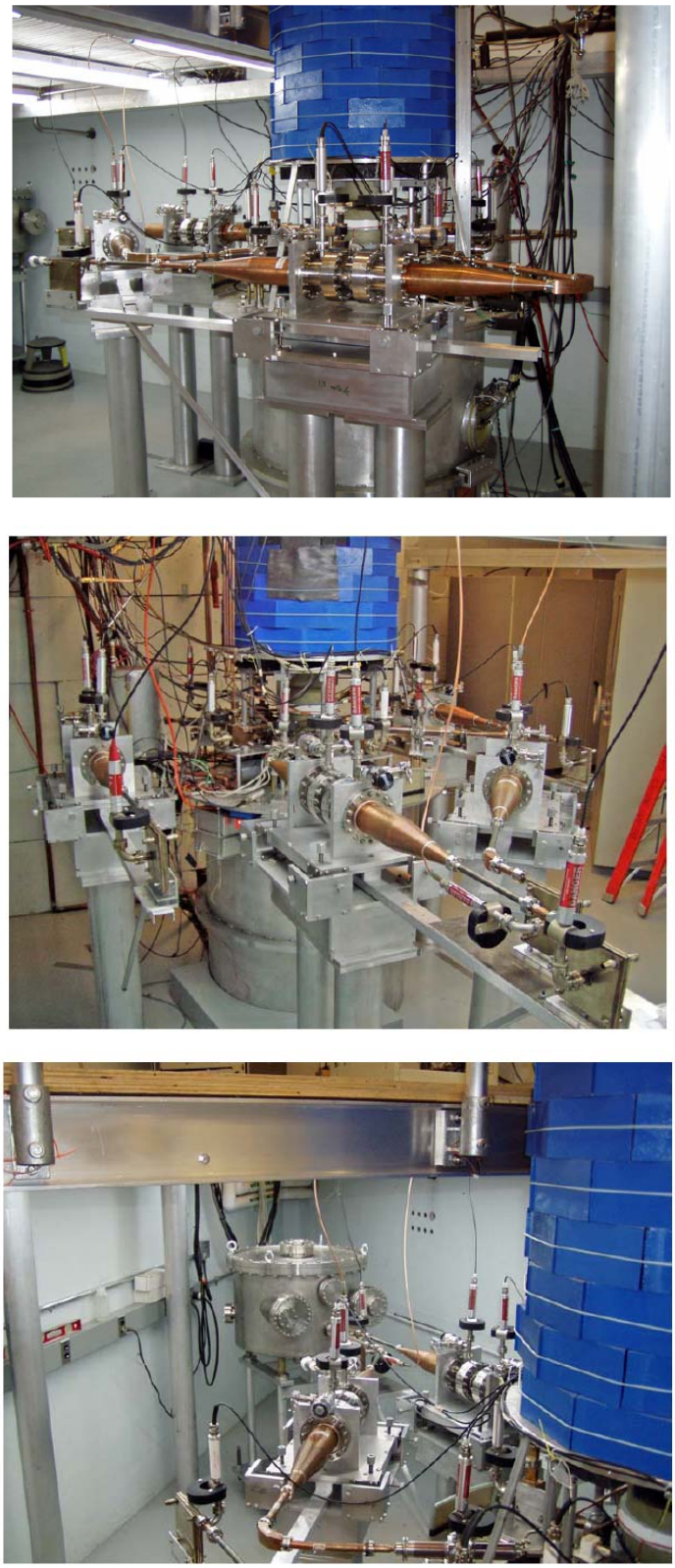

Fig. 1. Photographs of Omega-P 34-GHz magnicon, with windows and transmission lines.

Full specifications for the Omega-P 34-GHz magnicon are given in Table I.

Table I. Design parameters for the Omega-P 34-GHz magnicon.

operating frequency	34.272 GHz
power output	44-48 MW
pulse duration	1.0-1.5 μsec
pulse repetition rate	10 Hz
Efficiency	41-45%
drive frequency	11.424 GHz
drive power	150 W
Gain	54 dB
beam voltage	500 kV
beam current	215 A
gun perveance	0.61×10^{-6} AV$^{-3/2}$
beam diameter	0.8-1.0 mm
magnetic field, deflecting cavities	13.0 kG
magnetic field, output cavity	22.5 kG

III. PRELIMINARY RESULTS

Omega-P's Phase I program was devoted to development of several quasi-optical pulse compressor designs for operation at 34.272 GHz. Since first introduced for SLC, RF pulse compressors with steadily improving parameters have continued to be developed. Most recently, a dual-mode, dual delay line SLED-II type pulse compressor demonstrated 4:1 compression with a peak rf power of >500 MW at X-band [7]. The concepts enshrined in that S- and X-band RF pulse compression work have informed the Ka-band work recounted here.

Preliminary tasks which have been successfully completed include:

1. refinements in designs of passive and active quasi-optical passive compressors;
2. study of several diffraction grating designs for use as active elements for a quasi-optical pulse compressor;
3. study of a prototype quasi-optical active pulse compressor, using an active grating; and
4. development of specialized components needed for realization of practical pulse compressors operating at 34.272 GHz.

In the course of accomplishing these tasks, two versions of quasi-optical passive compressors were fabricated and tested experimentally. The first version embodies a three-mirror resonator, while the second embodies a four-mirror resonator. Both resonators have a diffraction grating as the coupling device. Theoretical and experimental investigations which have been performed show that the four-mirror passive compressor is the most promising. In addition to favorable operating parameters, the four-mirror resonator can be easily extended to become a passive multi-resonator compressor, which is the quasi-optical equivalent of a conventional SLED-II system that employs shorted waveguide delay lines. Use of a multiple-resonator quasi-optical system allows for generation of a near flat-top output pulse, rather than the rounded pulse

characteristic of SLED, for example. The four-mirror design also provides the possibility for testing electrically-controlled diffraction gratings to be used in active quasi-optical compressors or active quasi-optical delay lines (e.g., active SLED-II) [8].

Design calculations, fabrication, and testing of an electrically controlled diffraction grating were also carried out. An active quasi-optical compressor using this grating was demonstrated. At low power levels, a power gain of seven-to-one was obtained with this arrangement. The low-power studies conducted established the validity of the concepts proposed, both for passive and active pulse compressors. But practical utility for these concepts will clearly require development and testing of high-power designs to operate at input power levels of 10-40 MW, to provide >100 MW compressed output pulses of ~100 ns pulse width at 34.272 GHz.

IIIa. Three-mirror quasi-optical passive compressor

The first version of a quasi-optical passive compressor consists of a high-*Q*-factor three-mirror resonator, and an excitation system. This arrangement is diagrammed in Fig. 2. The resonator consists of two focusing mirrors that provide a high-*Q*-factor operating eigenmode of the running-wave type, and the third mirror with a fine corrugation on its surface.

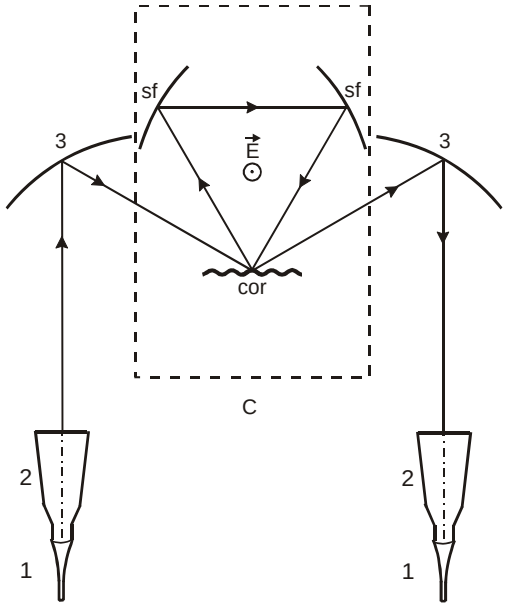

Fig. 2. Diagram of the three-mirror compressor with its excitation system studied during Phase I. *C* – resonator; *cor* – corrugated mirror; *sf* – focusing mirrors; *1* – rectangular to circular cross-section transducer; *2* – horn converting TE_{11} mode into Gaussian wavebeam; *3* – feed mirrors.

The corrugated mirror provides coupling of the operating mode with the wave beam formed by the excitation system. The coupling with the resonator is provided by using the -1^{st} diffraction maximum of the grating, as depicted in Fig. 3. The required period of the grating is determined by the expression

$$d = \frac{2\pi}{k(\sin\theta + \sin\theta_{-1})}, \qquad (1)$$

where θ is angle of wave beam incidence on the grating measured from the normal, and θ_{-1} is angle corresponding to the -1^{st} diffraction maximum. The corrugation amplitude should be chosen based on the necessity to provide the required Q-factor of resonator coupling.

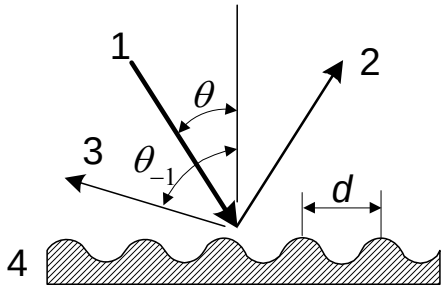

Fig. 3. Diagram to show scattering into two beams from one (*1*) incident on the diffraction grating (*4*), namely, the mirror beam (*2*), and the -1^{st} diffraction maximum beam (*3*).

An important feature of the three-mirror resonator is that, since it is essentially a ring resonator, it provides no reflection of power back to the source. Therefore, input to the resonator does not require an additional 3-dB coupler, as does a SLED compressor. The structure of the field for the operating mode of the resonator was calculated using the well-known Fox-Li method described in [9].

In order to have the highest resistance to RF breakdown, the polarization of the electric field in the resonator is chosen with the component normal to the surfaces of all the mirrors small, tending to zero as the mirror apertures increase. The mirror dimensions are chosen to provide a level of diffraction losses below the level of Ohmic losses. The minimum transverse mirror dimensions are estimated basing on the expression for the Fresnel parameter

$$N_F = \frac{ka^2}{L} \geq 2\pi, \tag{2}$$

where a is diameter of the mirrors, and L is optical length of the resonator. The excitation system includes a horn that converts the main mode of standard rectangular waveguide into a Gaussian beam, and a pair of matching mirrors. Those mirrors provide a distribution of the field which is close to the transverse distribution of the field of the operating mode (the lowest TEM_{00n} mode) over the face of the corrugated mirror of the resonator. The radiation at the compressor output is focused again into the single-mode waveguide, using a second set of components as for input coupling.

IIIb. Optimization of the three-mirror passive compressor parameters

Below we outline a calculation of pulse compressor parameters (compression ratio and efficiency), as they depend on the resonator Q-factor and the form of the phase modulation of the input pulse. Note that the SLED compressor uses for phase modulation a rapid step-wise variation with a phase shift of 180° one compressed pulse width τ before the end of the input pulse. This rapid phase shift places a bandwidth requirement on the high-power amplifier (klystron, in the case of X-band SLED-II). However, the 34-GHz magnicon bandwidth is relatively narrow (~ 20 MHz), so that imposition of a rapid phase shift of 180° at the magnicon input would result in an

undesirable ~100 ns notch in output power. As a result, linear frequency modulation across the full input pulse is much more appropriate, as it shall be shown that this does not require nearly as large a bandwidth.

Compressor efficiency is defined as the ratio of the output pulse energy to the pulse energy at the compressor input, namely

$$\eta = \frac{\int_{t_n}^{t_n+\tau} |E_{out}|^2 dt}{\left(|E_{in}|^2\right)_{\max} T} \tag{3}$$

where E_{in} and E_{out} are complex amplitudes at the input and output of the compressor, t_n is time at which the pulse starts to fill the accelerating structure $T = \int_{-\infty}^{+\infty} |E_{in}(t)|^2 dt \Big/ \left(|E_{in}|^2\right)_{\max}$ is duration of the input pulse, , and τ is time of filling of the accelerating section. The pulse compression ratio s is

$$s = \frac{T}{\tau}, \tag{4}$$

the ratio of duration of the input and output pulses. The power gain ratio is given by

$$P_g = s\eta, \tag{5}$$

the ratio of the power of the output pulse averaged over the time of filling of the accelerating structure to the peak power of the input pulse, e.g.

$$P_g = \frac{\int_{t_n}^{t_n+\tau} dt |E_{out}|^2}{\tau |E_{in}|^2} \ . \tag{6}$$

For most accelerator applications, a flat-top compressed output pulse is desired. However, for component testing, breakdown and surface fatigue studies, a rounded pulse is acceptable.

Transfer from input to output of a microwave pulse of complex amplitude of the form $e(t) = E(t)\exp(i\omega_g t)$ with smooth modulation in phase is described by the following equation:

$$\frac{dE_{out}(t)}{dt} + i\left[\omega_o{}'\left(1+\frac{i}{2Q_{ext}}\right) - \omega_g\right]E_{out}(t) = \frac{dE_{in}(t)}{dt} + i\left[\omega_o{}'\left(1-\frac{i}{2Q_{ext}}\right) - \omega_g\right]E_{in}(t), \tag{7}$$

where Q_{ext} is the external Q-factor of the resonator and ω_0' is eigenfrequency of the resonator. Eq. 7 is to be integrated for a pulse with linear frequency modulation given by formula:

$$\begin{cases} e_{in}(0 \le t < T) = exp\left[i\left(\omega_g t + \mu t^2/2\right)\right], \\ e_{in}(t < 0,\ t \ge T) = 0. \end{cases} \tag{8}$$

where μ is parameter that measures the frequency modulation. In this case the efficiency is a function of the dimensionless parameters: $\alpha = \dfrac{\mu T^2}{2}$, $\beta = \left(\omega_0' - \omega_g\right)T$, $\gamma = \dfrac{\omega_0' T}{2Q_{ext}}$ and s.

Fig. 4 shows optimized efficiency and power gain coefficient as functions of the compression ratio s. Optimized parameters that correspond to point **A** in Fig. 3 (f_0 = 34.272 GHz, s = 4, η = 65.89%, and P_g = 2.64) are $\alpha = 11.78$, $\beta = 8.61$, $\gamma = 2.11$. Efficiency of compression in the case of linear modulation is seen to be about 10% lower than the case of step-wise modulation. Table 1 lists dimensionless compression parameters that correspond to point **A** in Fig. 3 for various durations of the input pulse.

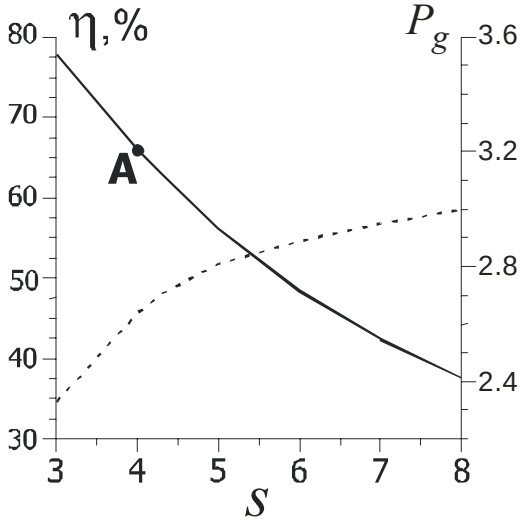

Fig. 4. Efficiency η (solid line) and power gain P_g (dashed line) of optimized passive compressors with linear frequency modulation.

Table 1. Optimized parameters corresponding to point A in Fig. 5.

T, ns	τ, ns	$\Delta f_0'$, GHz	Q_{ext}	Δf_g, GHz
500	125	0.003	25,516	0.007
100	25	0.014	5,105	0.037
80	20	0.017	4,084	0.049

Both the frequency modulation $\Delta f_o'$ and initial detuning Δf_g are seen to be in the range of a few 10's of MHz. With a rectangular input pulse having gentle linearly-varying FM, the optimum parameters found gave efficiency with s = 4 of η = 66%, and a total frequency modulation required for a 500 ns input pulse of only 2.74 MHz is required, a value well within the ~20 MHz bandwidth of the 34-GHz magnicon.

Fig. 5 shows calculated dependencies of the power of the output P_{out} and input P_{in}, power pulses as functions of dimensionless time, $t_0 = t/T$ for point **A** in Fig. 4.

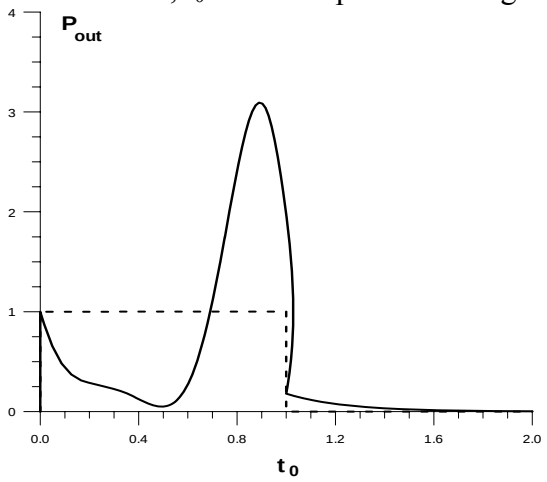

Fig. 5. Power of the output pulse (solid line) and of the input pulse (dashed line) as functions of dimensionless time, $t_0 = t/T$ corresponding to point **A** in Fig. 5.

IIIc. Prototype of a passive compressor with a three-mirror resonator

For the above design calculations for the three-mirror resonator to be tested in the laboratory at low power, the following parameters were chosen: frequency f_0 = 34.272 GHz, output pulse duration τ = 20 ns, and compression ratio s = 4. The optimal loaded Q-factor of the resonator should be ~ 4,000. Results of calculated dimensions of focusing mirrors, the corrugated mirror, and the distance between the mirrors, as well as the results of measuring the unloaded and loaded Q-factor of the resonator are listed in Table 2. The resonator mirrors had different dimensions in the plane shown in Fig. 3 (plane ||) and the plane perpendicular to it (plane ⊥).

Table 2. **Mirror dimensions in plane || and plane ⊥ and resonator parameters.**

transverse dimensions of the focusing mirrors, mm	|| = 227, ⊥ = 150
radii of curvature of the parabolic mirrors, mm	|| = 5313.7, ⊥ = 796.5
transverse dimensions of the corrugated mirror, mm	|| = 224, ⊥ = 110
corrugation period, mm	6.79
corrugation amplitude, mm	0.9
distance between the centers of the parabolic mirrors, mm	270.38
distance between the centers of the plane and parabolic mirrors, mm	320
frequency, GHz	34.272
loaded Q-factor (experimental)	4,200
unloaded Q-factor (experimental)	72,000

A general view of the experimental three-mirror passive compressor is shown in Fig. 6.

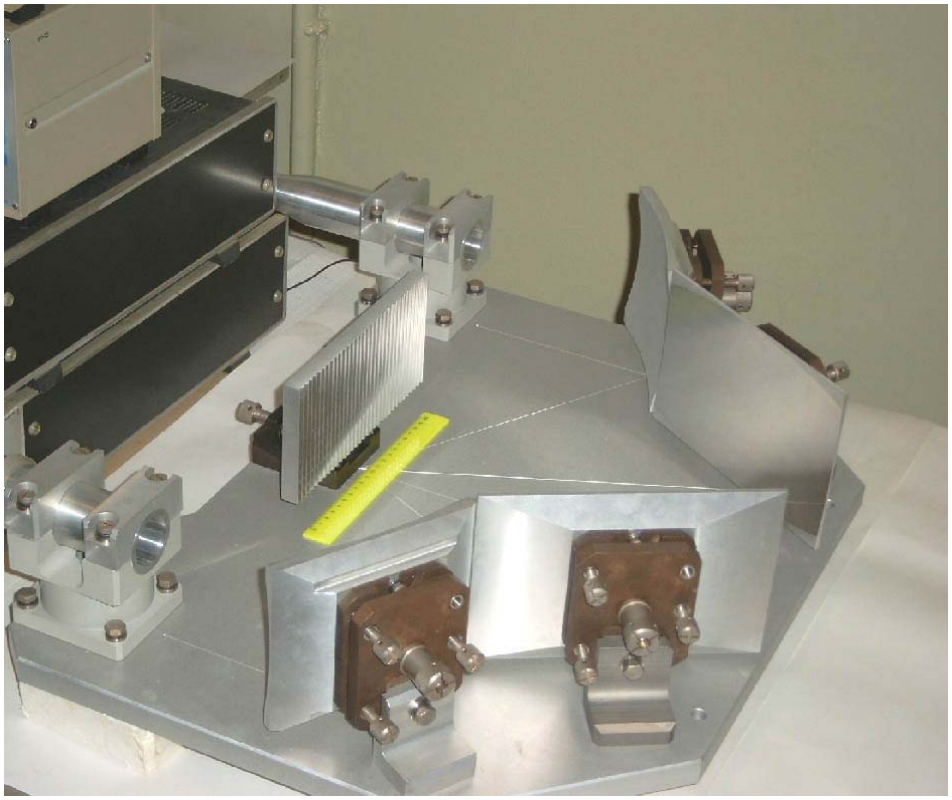

Fig 6. General view of the three-mirror passive compressor at 34.272 GHz.

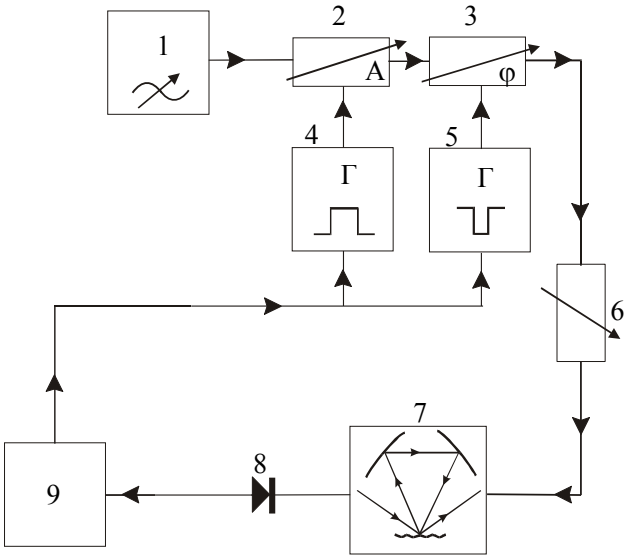

Fig. 7. The scheme of the experimental setup in the case of the step-wise frequency modulation. *1* - microwave generator; *2* - electrically controlled amplitude modulator on the p-i-n diode; *3* - electrically controlled phase rotator on the p-i-n diode; *4, 5* - pulse generators; *6* - high-precision attenuator; *7* - analyzed resonator; *8* - detector; *9* - oscilloscope.

The manufactured prototype of the compressor was tested at a low power level both in the scheme with step-wise frequency modulation, and that with linear frequency modulation. In the case of step-wise frequency modulation the compressor was tested in the setup shown in Fig. 7. A high-stability ($\Delta f/f = 10^{-5} - 10^{-6}$) klystron-type pulse generator was used as a source of input microwave pulses. The source worked in the regime of generation of rectangular pulses $\tau = 80 - 120$ ns. An electrically controlled amplitude modulator using a p-i-n diode was used. For the step-wise frequency modulation we used an electrically controlled phase rotator based on a p-i-n diode with its phase switching time $\tau_s \sim 1$ ns to switch the phase from 0 to 180°. An oscillogram of the compressed pulse obtained in that experiment is shown in Fig. 8. For a length of the input pulse 80 ns, $s = 4$, and $P_g = 3$, the observed efficiency of compression was 75%, which is essentially the same value as the efficiency of the SLED compressor at the same compression ratio.

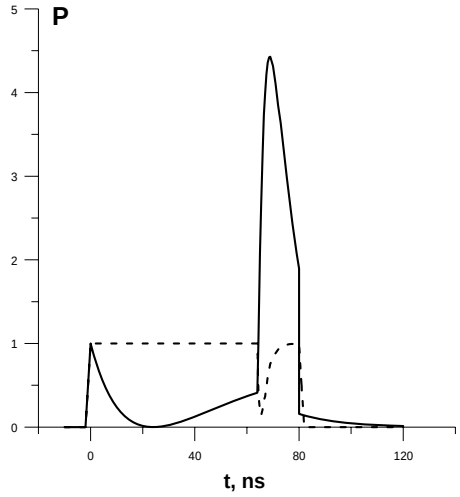

Fig 8. Oscillogram of the input and output pulses in the case of step-wise phase modulation: $T = 80$ ns, s = 4, $\eta = 75\%$, $P_g = 3$.

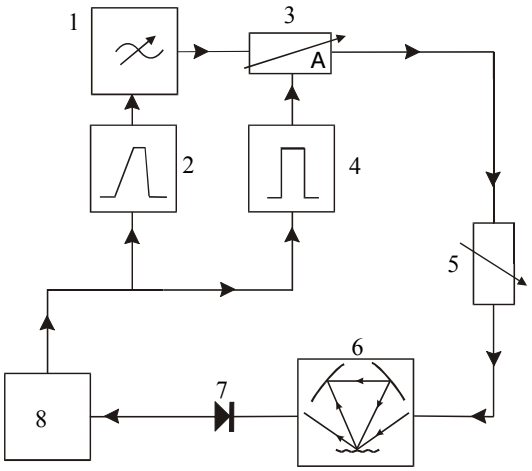

Fig. 9. The scheme of the experimental setup in the case of the linear frequency modulation. *1* - microwave generator; *2* – pulse generator; *3* – amplitude modulator; *4* - pulse generator; *5* - high-precision attenuator; *6* - analyzed resonator; *7* - detector; *8* - oscilloscope.

In the second set of experiments we tested the compressor with linear frequency modulation. Following the optimal dimensionless parameters found in Sec. 6c, frequency tuning within a pulse should be ~ 47 MHz, and detuning of the resonator relative to the pulse frequency should be ~17 MHz. In the case of the linear frequency modulation the compressor was tested in the setup shown in Fig. 9. The block diagram of the experimental setup included several generators: the Gunn-diode microwave generator with a built-in varicap (*1*), the generator of pulses with controlled shapes to control the frequency of the microwave generator by sending a voltage pulse to the varicap (*2*), the electrically controlled former of the envelope of microwave pulses (*3*), and the generator feeding the envelope former (*4)*. The required rate of frequency tuning to create the necessary linear frequency modulation was achieved by setting the corresponding rate of voltage build-up in the controlling pulse of generator (*2*). In this case, separate calibration of the dependence of the frequency of the microwave generator (*1*) on the voltage applied was taken into account. The optimal initial frequency detuning from the resonant frequency was sought directly during the experiment by means of varying the constant component of the pulse amplitude in generator (*2)*.

Samples of the oscillograms of the output pulses obtained in this variant of compressor operation are shown in Fig. 10 for two input pulse durations. In Fig. 10a the input pulse is 100 ns long, whilst in Fig. 10b it is 80 ns long. Experimental parameters are listed in Table 3.

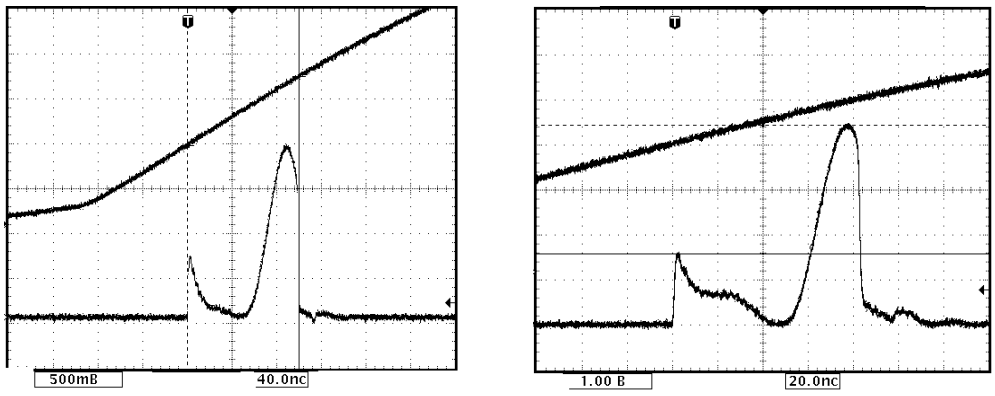

(*a*) (*b*)

Fig 10. Oscillograms of the output pulse in the case of linear frequency modulation:
(a) T = 100 ns, Δf_g = 39.3 MHz, s =3.6, η = 65%, P_g=2.34;
(b) T = 80 ns, Δf_g = 51 MHz, s = 4, η = 59%, P_g=2.36.

Table 3. Compression with linear frequency modulation: experimental data

T (ns)	Δf_g MHz	S	η (%)	P_g
120	19.4	3	58	1.74
120	28.6	3	71	2.13
110	33.2	3.5	62	2.17
100	39.3	3.6	65	2.34
90	45.4	3.7	65	2.41
80	51.0	4	59	2.36

For a compression ratio s = 3, compressor efficiency is ≈ 70%, and power gain is ≈ 2.13. When the compression ratio is s = 4, compressor efficiency is ≈ 60%, and power gain is ≈ 2.4. Thus, the experiment performed showed that the developed three-mirror quasi-optical resonator makes it possible to compress pulses with linear frequency modulation with efficiency close to the theoretical limit. However, power gain is seen to be lower than in the case of the step-wise frequency modulation. It should be noted that the passive compressor composed of two quasi-optical resonators fed with a pulse with linear frequency modulation makes it possible to increase the power gain and exceed the SLED system parameters [10].

IIId. Four-mirror quasi-optical passive compressor

In the three-mirror resonator (Figs. 2 and 6), the system for resonator excitation that consists of horns and feeding mirrors is situated in the plane in which the wave in the ring resonator propagates. This design restricts selection of the dimensions of the resonator mirrors, since the focusing mirrors block the beam incident from the feeding mirror of the excitation system. To overcome this limitation, a four-mirror resonator has been developed, wherein the excitation system is situated in the plane perpendicular to the plane of circulation of the beams in the resonator. A diagram of the four-mirror resonator configuration is shown in Fig. 11.

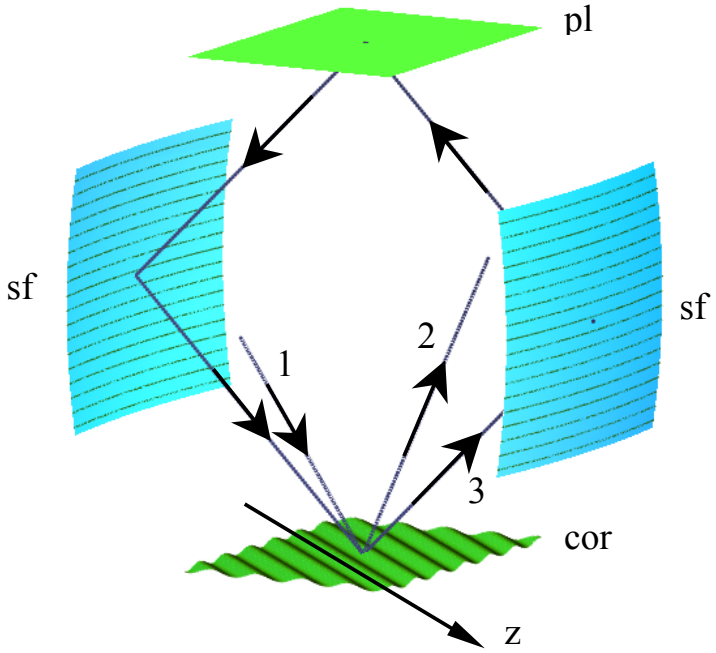

Fig. 11. Schematic diagram of the four-mirror compressor.
cor – corrugated mirror; *sf* – focusing mirrors; *pl* – plane mirror; *1*- incident beam;
2 – mirror beam; *3* - the -1^{st} diffraction maximum.

This design of the quasi-optical resonator makes it possible to use it to create passive multi-resonator compressors, in order to increase the power gain and compression efficiency [10,11], as well as a quasi-optical equivalent of the SLED-II system based on a mirror delay line to achieve a flat-top output pulse. It should be noted that TE and TM modes have different reflection

coefficients from the diffraction grating. Therefore, for a resonator with a diffraction grating it is important that these modes should be eigenmodes of the resonator. Only a resonator with an even number of mirrors satisfies this condition. In the four-mirror resonator that has been studied during Phase I, the operating mode is the TEM_{oon} or *E*-polarization mode ($H_z = 0$), which has a high breakdown-level polarization relative to the grating. The resonator is excited also with a wave beam with linear *E*-polarization ($H_z = 0$). The angles of incidence of the wave on the mirrors and the grating are 45°. Direction of the corrugation also forms the angle of 45° to the main symmetry planes.

IIIe. Prototype of a passive compressor with a four mirror resonator

To carry out design calculations for a four-mirror resonator, parameters as for the three-mirror resonator where chosen, namely radiation frequency $f_0 = 34.272$ GHz, duration of the output pulse $\tau = 20$ ns, and compression ratio $s = 4$. The design layout of the four-mirror resonator is shown in Fig. 12. The compressor has an excitation system consisting of two horns and two feeding mirrors. The resonator is formed by two focusing mirrors, a plane mirror, and a corrugated one. Fig. 12a shows the position of the mirrors in the plane in which the excitation system is situated (plane ||), while Fig. 12b shows the position of the mirrors in the plane perpendicular to the plane of the excitation system (plane ⊥). The horn of the excitation system converts the TE_{10} mode of a rectangular waveguide into an axially symmetric, linearly polarized Gaussian beam turned to an angle of 55° relative to plane (||).

The results of calculating the dimensions of the focusing mirrors, corrugated and plane mirrors, distance between the mirrors, as well as the results of measuring the unloaded and loaded *Q*-factor of the resonator are listed in Table 4. Dimensions in the table are given in both planes.

Table 4. **Mirror dimensions in plane (||) and plane (⊥) and resonator parameters.**

transverse dimensions of the focusing mirrors, mm	|| –184, ⊥ – 223
radii of curvature of the parabolic mirrors, mm	|| –1018, ⊥ – 6003
transverse dimensions of the corrugated and plane mirrors, mm	|| –156, ⊥ – 221
corrugation period, mm	8.75
corrugation amplitude, mm	0.8
distance between the centers of the adjacent mirrors, mm	201.7
frequency, GHz	34.272
loaded *Q*-factor (experiment)	3,400
unloaded *Q*-factor (experiment)	50,000

The general view of the four-mirror passive compressor that was built for low-power tests is shown in Fig. 13.

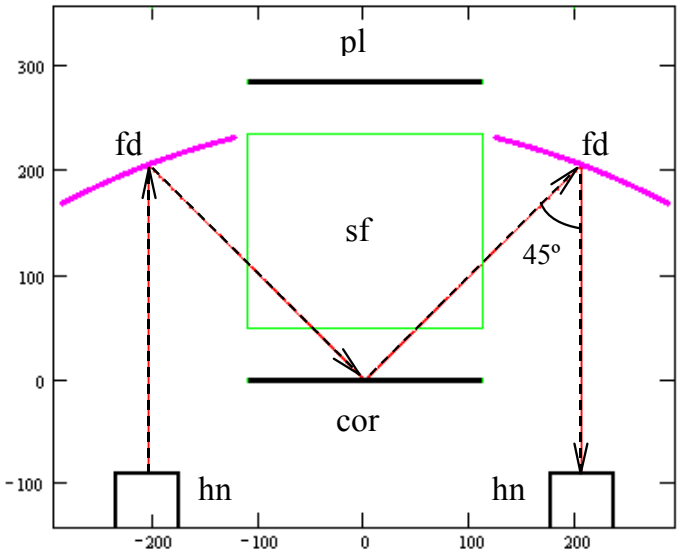

a)

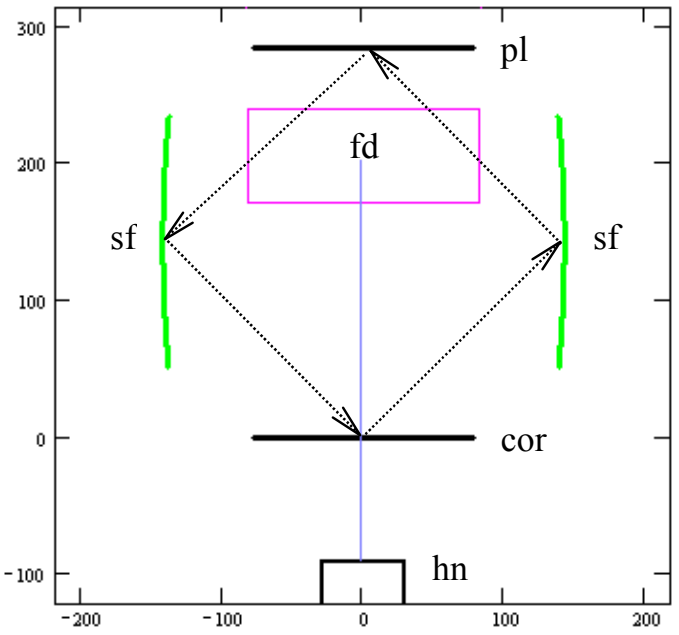

b)

Fig. 12. Schematic diagram of the developed four-mirror compressor with the excitation system: *cor* – corrugated mirror, *sf* – focusing mirrors, *pl* – plane mirror, *fd* – feeding mirror, *hn* – horn.

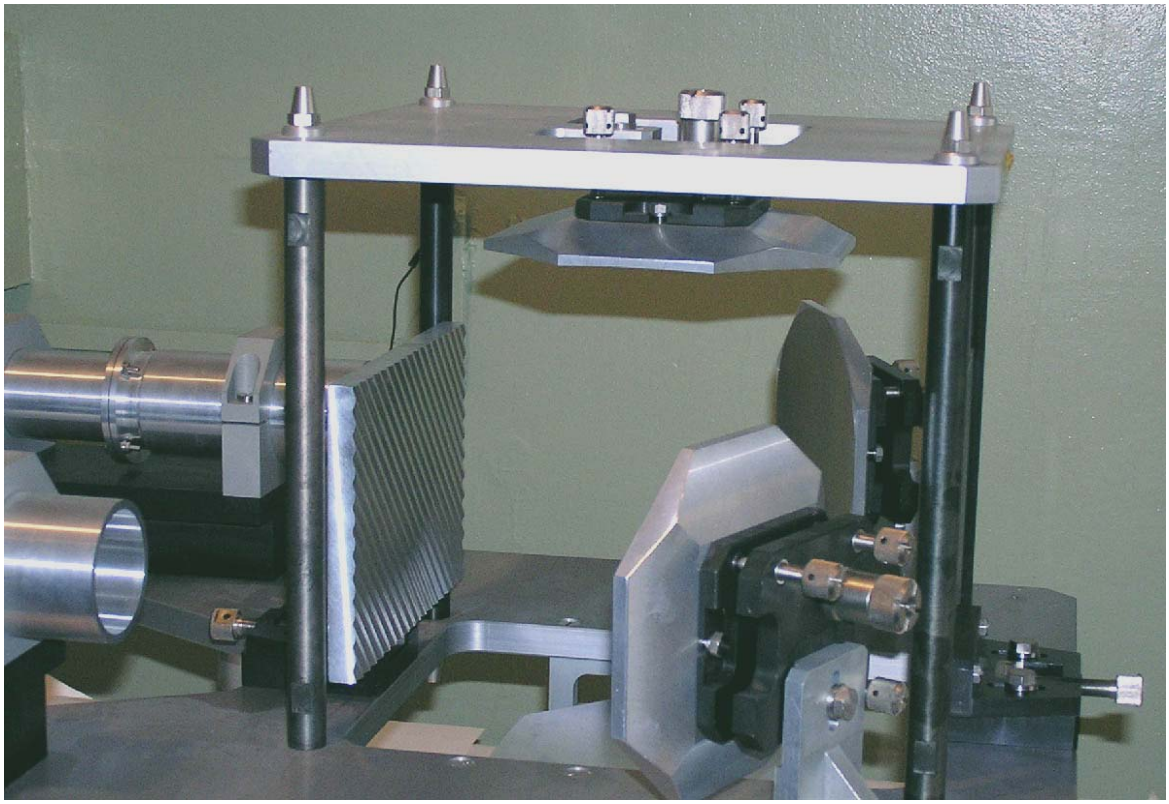

Fig. 13. General view of the four-mirror passive compressor at 34.272 GHz.

According to numerical calculations using the Fox-Li method, the eigenmode of the four-mirror resonator is a Gaussian beam (with purity 99.7%), the transverse cross-section of which is elliptical, and which has a plane phase front near the grating. The intensity level e^{-1}-width of the beam in plane ($\parallel$) is 42 mm, and in plane ($\perp$) is 21 mm. The resonator is driven by an excitation system radiating an axially symmetric Gaussian beam, with a plane phase front near the diffraction grating to match the resonator mode. The intensity level e^{-1}-width of this beam is 30 mm.

The unloaded and loaded Q-factor of the resonator were measured using the same equipment as in the case of the three-mirror resonator. The Q-factors of the resonator were determined in the experiment with a long rectangular pulse at the resonance frequency, as shown in Fig. 14. The loaded Q-factor was found from the rate of the relaxation of the energy of the excited resonator. The unloaded Q-factor and the coupling Q-factor were separated by comparing the values of power at the stationary interval of the output pulse with the resonator turned on and off by means of inserting an ideal absorber inside. The measurements made it possible to determine the coupling Q-factor to be $Q_e \approx 3{,}650$, and unloaded Q-factor, to be $Q \approx 50{,}000$.

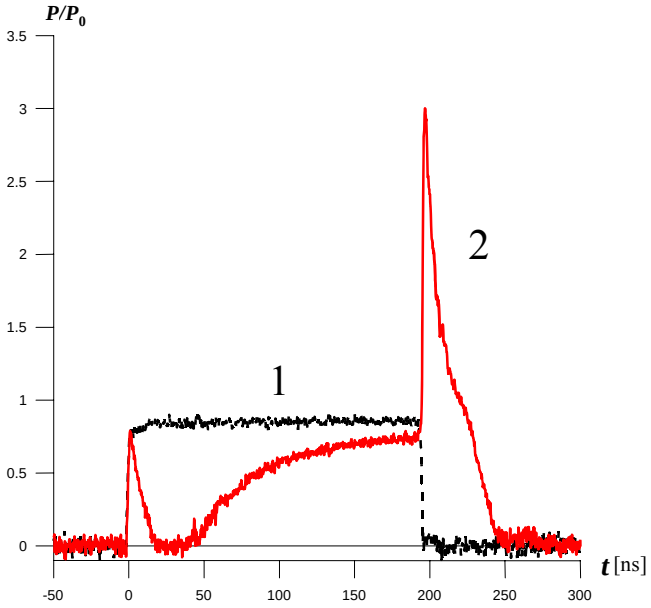

Fig. 14. Experimental oscillograms of output pulses: *1* – in case the cavity is switched off (filled by absorber), *2* – in case the cavity is switched on (without absorber).

The prototype of the passive four-mirror compressor was tested at a low power level both in the scheme with step-wise frequency modulation, and that with linear frequency modulation. In the case of the step-wise frequency modulation the compressor was tested in the setup similar to that shown in Fig. 7. The oscillogram of the compressed pulse obtained in this experiment is shown in Fig. 15.

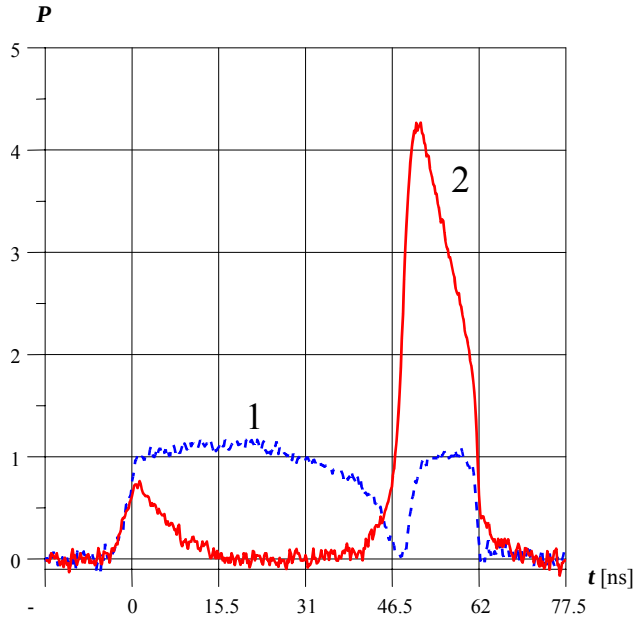

Fig. 15. Oscillogram of the input (*1*) and output (*2*) pulses in the case of step-wise phase modulation: $T = 62$ ns, $s = 4$, $\eta = 77\%$, $P_g = 3.08$.

In the second set of experiments the four-mirror compressor was tested with linear frequency modulation using the setup similar to that shown in Fig. 9. Samples of the oscillograms of the output pulses obtained in this experiment are shown in Fig. 16.

Experimental characteristics of compressed pulses and parameters of compressor operation are listed in Table 5.

TABLE 5. Experimental data for compression based on four-mirror resonator

T, ns	Phase modulation	S	η, %	P_g
62	Step-type	4	77	3.08
80	Chirped regime Δf_g =50 MHz	4	63	2.52
74	Chirped regime Δf_g =53 MHz	4	61	2.44

Thus, the experiments performed showed that the experimental four-mirror quasi-optical resonator makes it possible to compress pulses with linear frequency modulation with efficiency close to the theoretical limit. The measured compression efficiency and power gain of three-mirror and four mirror resonators are close to each other and are in good agreement with the calculated values. As it has been already stated, compression efficiency can be increased, in principle, by employing multi-resonator compressors. Specifically, a two-resonator compressor gives the possibility to increase the compression efficiency and power gain by about 10% at the same compression ratio. A possible variant for creation of a two-resonator compressor based on the developed four-mirror resonator is shown in Fig. 17.

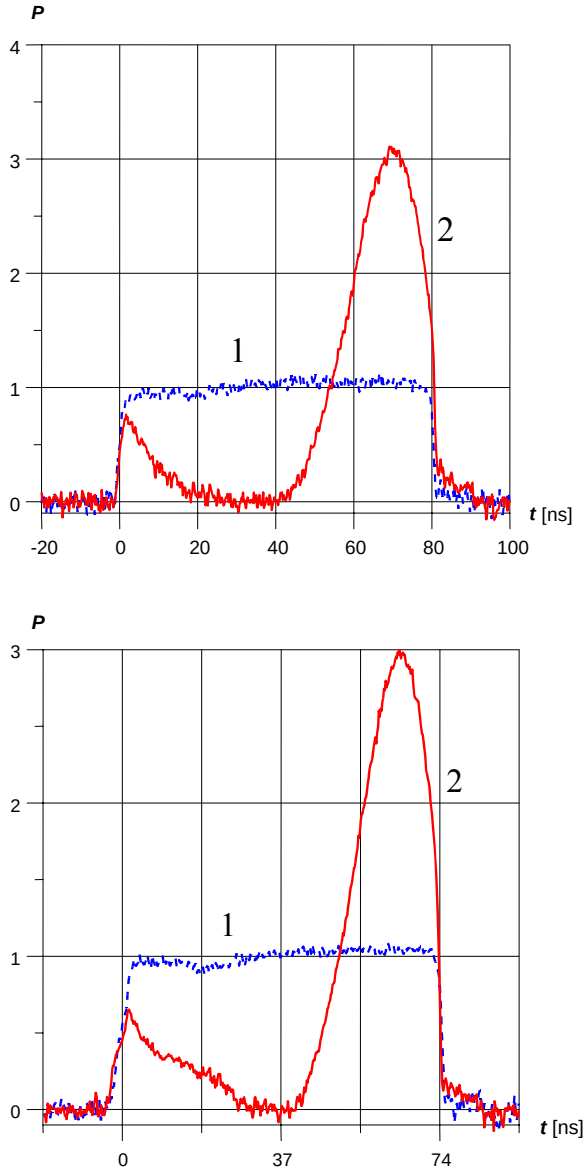

Fig.16. Oscillograms of the input (1) and output (2) pulses in the case of linear frequency modulation: *(a):* $T = 80$ ns, $\Delta f_g = 50$ MHz, $\eta = 63\%$; *(b)* $T = 74$ ns, $\Delta f_g = 53$ MHz, $\eta = 61\%$.

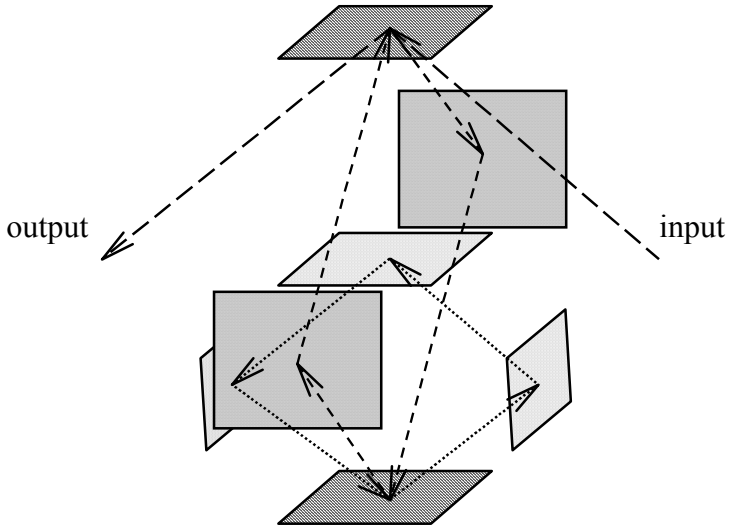

Fig. 17. Mirror arrangement for a passive two-resonator pulse compressor.

IIIf. Diffraction gratings as active elements for quasi-optical pulse compressors

Quasi-optical traveling-wave resonators with a diffraction grating as the coupling device, as have been described in previous sections, can be used in active microwave pulse compressors, as diagrammed in Fig. 18. To achieve this, the grating, in the regime of energy storage should provide scattering of only a small portion of the incident power into the diffraction (-1^{st}) beam, to couple the resonator with the feeding line, as shown in Fig.18a. Then, to switch out the stored energy, the grating should switch quickly into the state in which a significant portion of the power is scattered into the diffraction beam, as in Fig. 18b. As a result, the coupling of the resonator with the feeding line improves, and the energy stored in the resonator leaves the resonator in a short time. The switching can be done by changing properties of the diffraction grating, specifically by using gas-discharge tubes to change the distribution of the electromagnetic field on the grating, thus changing its electrodynamic structure.

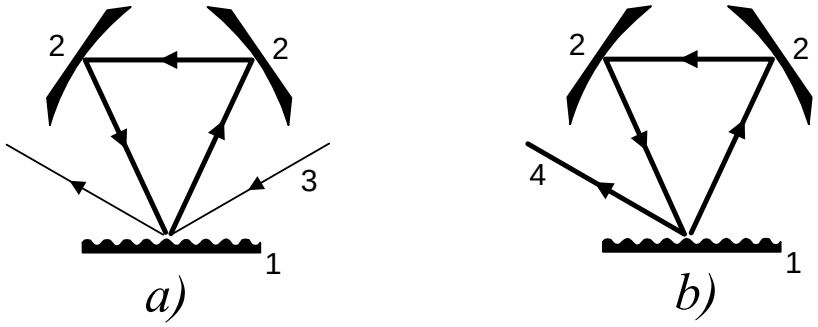

Fig. 18. Concept of compression basing on the quasi-optic resonator.
1 - diffraction grating/switch; *2* - focusing mirrors; *3* - input pulse; *4* - output pulse.
(*a*) - resonator in the regime of energy storage; (*b*) - in the regime of compressed output pulse.

Operation of such gratings was modeled by the FDTD method [12]. The calculation model is shown in Fig. 19. The reflecting diffraction grating was formed by a metal mirror (1) and a periodical structure over it (2). Distribution of electric and magnetic currents set in the plane (3) over the grating radiated a plane wave (4) towards the gratings. The wave interacted with the grating and branched into two waves: the mirror one (5) and the diffraction one (6) corresponding to the -1st maximum of the grating. To provide defense against electrical breakdown of the grating, we chose the TE polarization of the electromagnetic waves, at which the vector of the electric field is parallel to the grating grooves. In this case there is no noticeable increase of intensity of the electric field on the periodic structure.

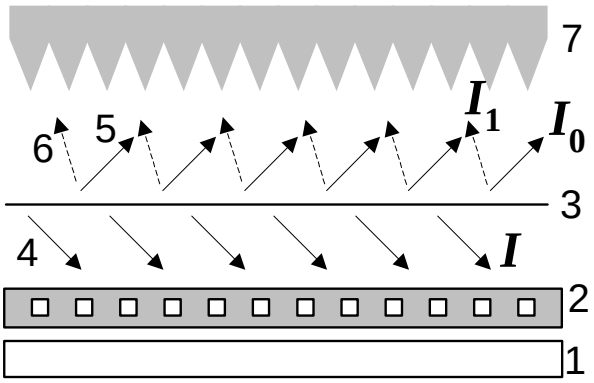

Fig. 19. Model for computation of a controlled diffraction grating: *1* - plane metal mirror; *2* - diffraction grating; *3* - plane with fixed currents launching a wave towards grating; *4* - wave incident on grating; *5* - reflected wave; *6* - diffraction wave (-1st maximum); *7* - absorber.

The calculations aimed at choosing the type and configuration of the grating that would provide almost total reflection (small scattering into the diffraction beam) in the absence of plasma in the switching elements, and at the lowest possible intensity of the electric field at these elements. We considered different types of gratings: those formed by dielectric tubes over a metal plane, by variously shaped metal profiles, by dielectric plates with gaps over a metal plane. Calculations revealed that it is unreasonable to use gratings that incorporate dielectric tubes, since the electric field becomes stronger at their side surfaces, which can result in development of multipactor discharges and poor electric reliability. The gratings that consist of a relatively thick dielectric plate with channels in it (which serve as gas-discharge tubes) seem to be more electrically reliable. The thickness of the plate is chosen such that the boundary between the vacuum and the dielectric is at the minimum of the electric field of the standing wave, as shown in Fig. 20a. As the result, appearance of a multipactor discharge is not very probable here. The intensity of the electric field in the channels is equal approximately to the intensity of the field in the standing wave. We calculated two versions of these gratings. In the grating of version *A* shown in Fig. 20, the channels are placed with a double period and have slightly different dimensions to provide weak scattering into the diffraction wave. In this case the reflection coefficient, equal to the ratio of intensity of the mirror wave to intensity of the incident one ($R^2 = I_0/I$), see Fig. 19, is close to unity. When plasma is produced, a strong periodic inhomogeneity appears in half of the channels, and a significant portion of the energy is scattered into the diffraction wave, as seen in Fig. 20b.

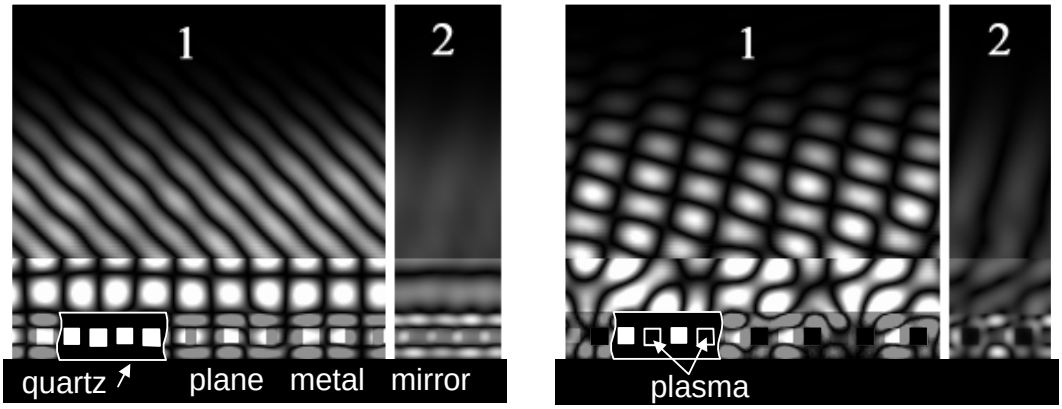

a) *b*)

Fig. 20. Distributions of the instantaneous electric field (1) and mean-square field (2) during reflection of the plane wave from the diffraction grating made of quartz: (*a*) - in the regime of energy storage in the resonator ($R^2 = 0.99$); (*b*) - in the regime of energy extraction from the resonator ($R^2 = 0.5$). In the figures the field within the quartz is shown in a darker color. The quartz structure with two grating periods is shown as black. The plasma inside the quartz is shown as black also.

In the grating of version *B* shown in Fig. 21, the channels are placed with wider period. To provide weak scattering into the diffraction wave, the grooves parallel to the channel were made on both surfaces of the dielectric plate. Without plasma the reflection coefficient of the grating is close to unity. When plasma is produced in each channel, a strong periodic inhomogeneity appears and a significant portion of the energy is scattered into the diffraction wave, as seen in Fig. 21b.

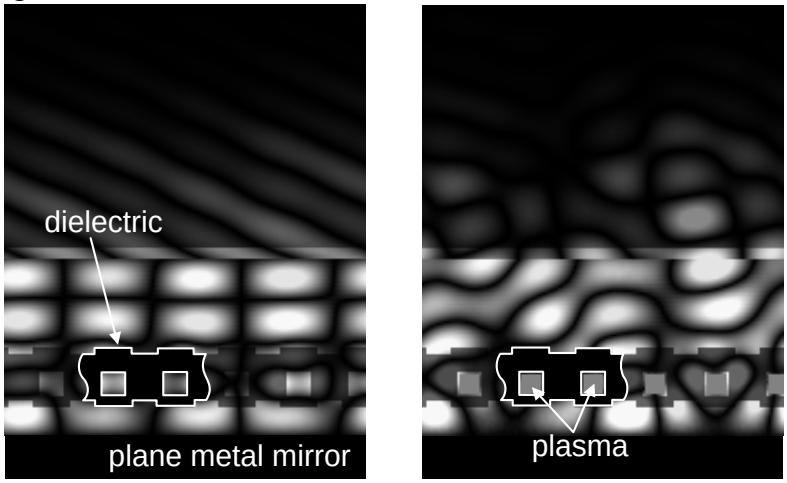

a) *b*)

Fig. 21. Distributions of the instantaneous electric field during reflection of the plane wave from the diffraction grating made of polystyrene: (*a*) - in the regime of energy storage in the resonator; (*b*) - in the regime of energy output from the resonator. In the figures the field within the dielectric is shown in a darker color. The part of polystyrene with channels is shown as black. The plasma inside the channels is shown as gray.

In the case of reflection from the grating made of quartz, which has a low value of Ohmic losses ($\tan\delta \approx 3\times10^{-4}$), the coefficient of power losses is $\alpha \approx 0.6\%$. Hence, the Q-factor of the resonator associated with those losses will be $Q \approx 120{,}000$ for a length of the beam run along the resonator of ~1 m. Therefore, the losses in quartz will not diminish the Q-factor of the storage resonator significantly. Technically, manufacture of the quartz grating that has been described is comparatively costly and time-consuming. That is why in order to check experimentally the possibility to create a controlled diffraction grating, design calculations were carried out for a grating made of polystyrene, which is shown in Fig. 23.

The parameters of the grating consisting of a dielectric plate and a metal mirror depend on the distance between the dielectric plate and the mirror. Therefore, for all such gratings we calculated optimal distances, at which the grating provided the necessary reflection coefficient. Fig. 22 shows the calculated dependence of the reflection coefficient from the version *B* grating as a function of the distance between the dielectric plate and the metal mirror in the absence of the plasma in the channels and after discharge ignition.

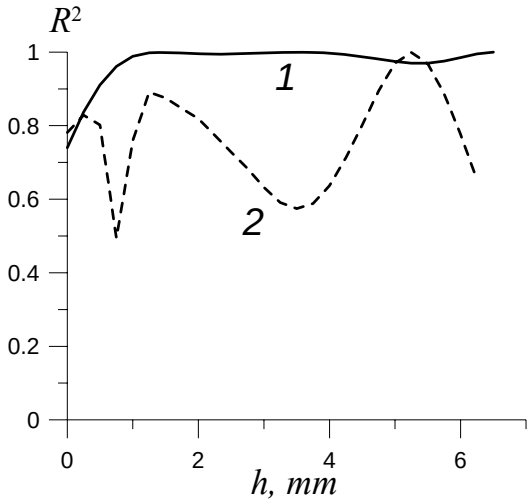

Fig. 22. Calculated dependence of the reflection coefficient from the version *B* grating, as a function of the distance *h* between the dielectric and the metal mirror, in the absence of plasma in the channels (1) and after plasma ignition (2).

IIIg. Study of quasi-optical three-mirror active compressor

At the preliminary stage of investigations, a version *A* grating made of polystyrene, with dimensions 50×25 cm^2 was manufactured and tested. Tests of such a grating showed that the time of switching was ~100 ns, which is too long to obtain compressed pulses that are to be several 10's of nanoseconds long. Therefore an important goal of the program was to develop a grating with smaller dimensions for providing a shorter switching time.

To address this goal, we designed and manufactured the polystyrene grating of version *B* with dimensions 26×11 cm^2. The dimensions of the grating were chosen such to allow it to fit into the three-mirror resonator described above as its active element. The general view of this

electrically controlled grating made of polystyrene and used in the experiments at low power levels is shown in Fig. 23. The shape of the grating can be seen in Fig. 23a, which shows a side-view photo of the grating without electrodes. This grating is made of two sheets of polystyrene with grooves in one of them, which communicate at one end, to pump the gas into and out of them. At the both ends of the grooves, metal electrodes are glued in, as shown in Fig. 23b.

Photographs of the experimental setup with the three-mirror resonator and a high-voltage generator for producing plasma discharges in the grating channels are shown in Fig. 24. Fig. 24b shows the illuminated grating at the moment of plasma production in the channels (*7* in Fig. 24b). The resonator is formed by two focusing mirrors (*1*) and the diffraction grating (*2*). The radiation is fed in and out of the resonator by means of horns (*3*) and matching mirrors (*4*). The voltage produced by the high-voltage pulse generator (*5*) was fed to the electrodes of the discharge channels via a set of ballast resistors (*6*). When high-voltage pulses are fed in, gas-discharge plasma (*7*) develops in the grating channels.

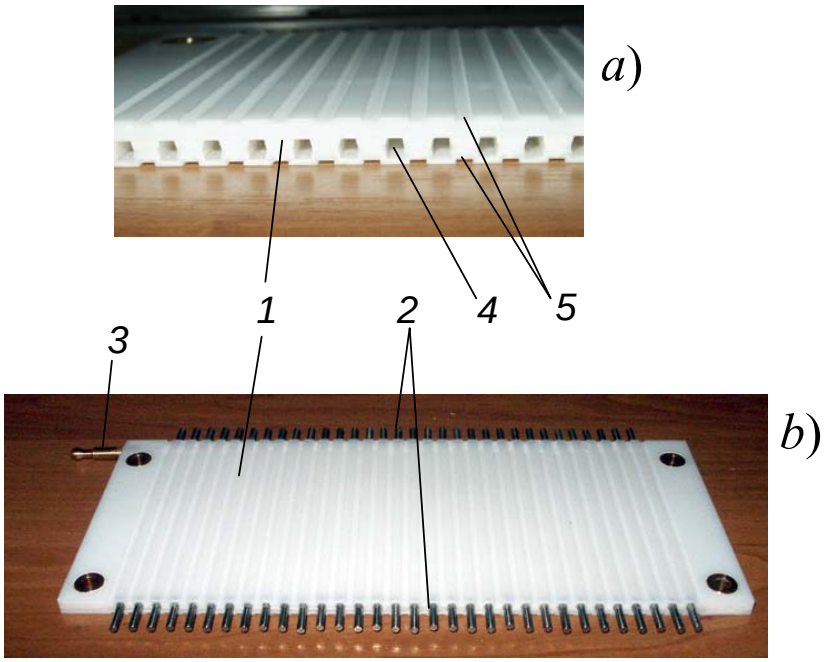

Fig. 23. General view of the polystyrene grating without electrodes (a) and with electrodes (b): 1 – polystyrene plate; 2 - electrodes; 3 – pumping port, 4 – channels, 5 – grooves.

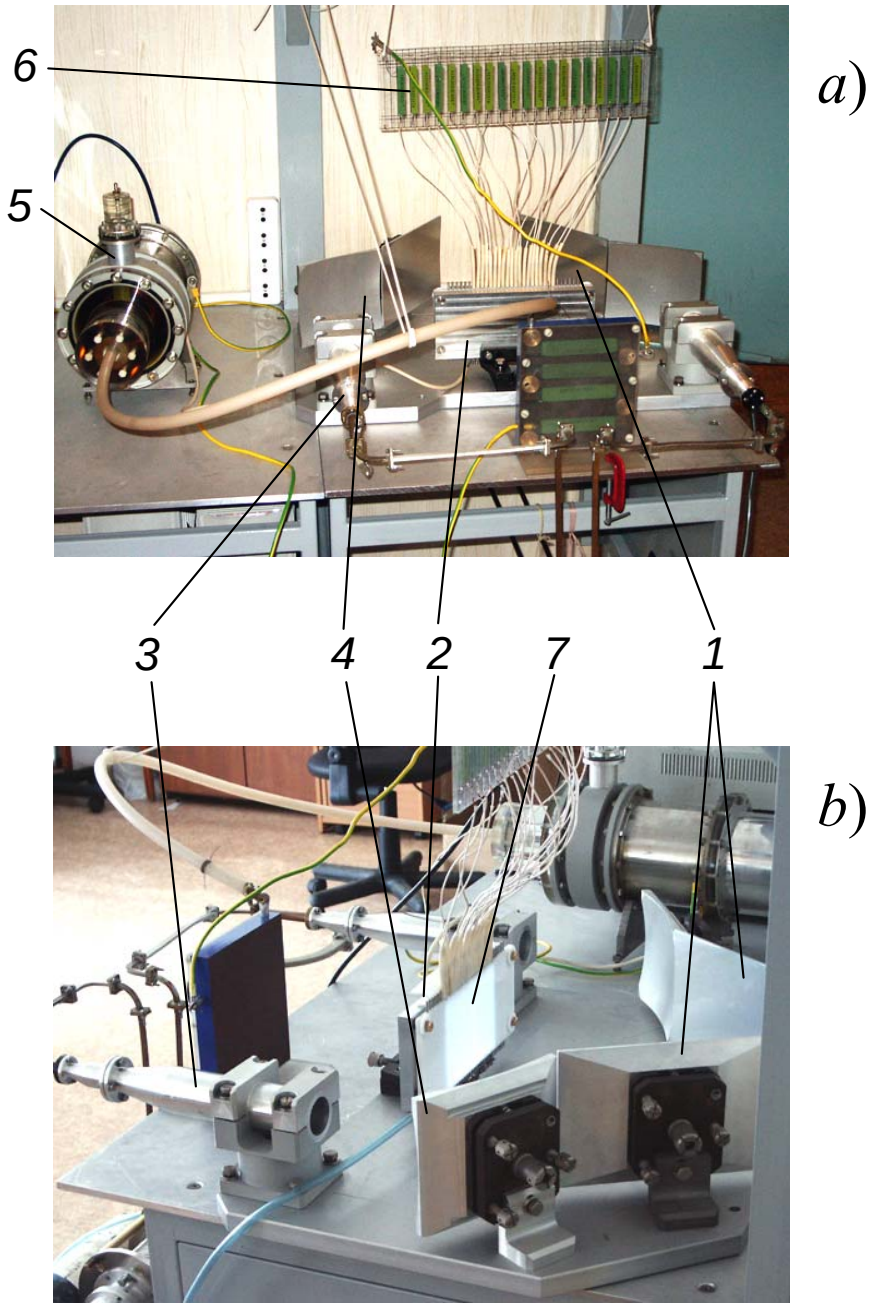

Fig. 24. Photographs of the quasi-optical three-mirror active compressor.
1 - focusing mirrors, *2* – diffraction grating, *3* – horn converting H_{11} mode into Gaussian wavebeam, *4* – feeding mirrors, *5* – high-voltage pulse generator, *6* - ballast resistors, *7* – gas-discharge plasma in channels of the grating.

A diagram of the experimental setup for studying operation of the quasi-optical three-mirror active compressor is shown in Fig. 25. The resonator (*1*) is excited by a low-power continuous-wave generator (*2*) at the frequency of 34.27 GHz. The voltage produced by the high-voltage pulse generator (*3*) was fed to the electrodes of the discharge channels via a set of ballast resistors (*4*). The radiation from the resonator output was sent to detector (*6*) via

attenuator (*5*), and then registered with a digital oscilloscope (*7*). In order to measure the frequency characteristics of the compressor, generator (*2*) was switched to the regime of frequency sweeping. The spectrum of the transmitted pulse was analyzed with a network analyzer (*8*), to which the radiation was sent via a directional coupler (*9*).

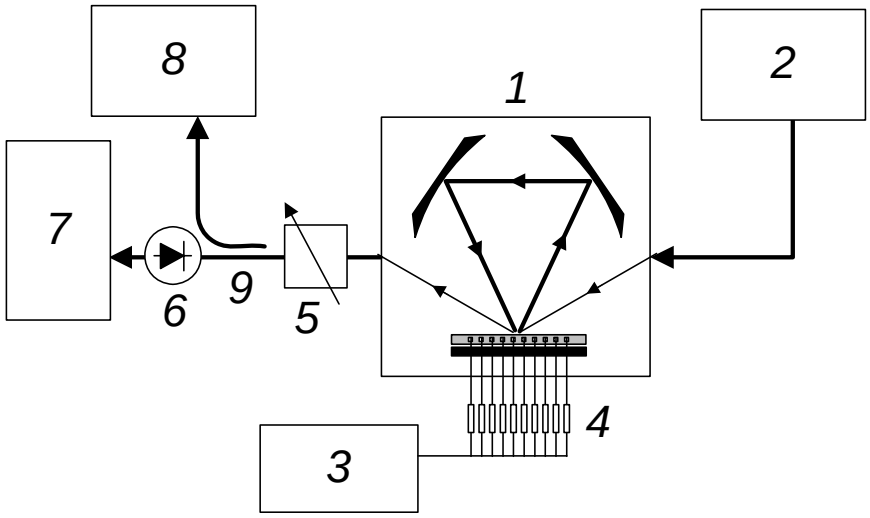

Fig. 25. Diagram of the experimental setup. *1* - quasi-optical three-mirror active compressor, *2* –- microwave generator, *3* – high-voltage pulse generator, *4* - ballast resistors, *5* – attenuator, *6* – detector, *7* – oscilloscope, *8* – network analyzer, *9* – directional coupler.

The design of the diffraction grating consists of a plane metal mirror and a dielectric periodic structure. This design makes it possible to control the coefficient of coupling of the resonator in the energy-accumulation mode with the exciting line by changing the distance between the polystyrene and metal plates h, as in Fig. 19. Therefore, the resonator was tuned by choosing distance h in such a way as to make the coupling between the resonator and the exciting line low. In this case the measured unloaded Q-factor of the resonator was $Q_0 = 28{,}000$. This relatively low Q-factor of the resonator is associated with the relatively high value of dielectric losses in polystyrene, for which the loss tangent is $\tan\delta \approx 10^{-3}$. When the dielectric grating is made of quartz, which has a much lower loss tangent, $\tan\delta \approx 3\cdot10^{-4}$, the losses in the dielectric will have little influence on the unloaded Q-factor of the resonator. Therefore, using a quartz grating we are able to obtain a higher Q-factor of the storing resonator. It should be noted that the unloaded Q-factor of a three-mirror resonator with a metal diffraction grating specially manufactured for such measurements and providing a low coupling coefficient has already been tested, and was found to be $Q_0 = 70{,}000$.

In the series of experiments performed, operation of the active compressor was studied when the resonator was tuned in such a way as to maximize the stored energy. This was achieved by making the distance between the polystyrene and metal plates of the grating such as to make the unloaded Q-factor of the resonator and the coupling Q-factor approximately equal. In this case the loaded Q-factor of the resonator in its energy-accumulation mode was $Q_L \approx$ 14,000, and the signal in the mirror beam (having passed through the resonator) at the resonance frequency was, not unexpectedly, weak.

To study the time of grating switching, the focusing mirrors of the resonator were covered with an absorber. In the absence of plasma in the channels, the intensity of the diffraction beam is low and the incident power is reflected into the mirror beam. The signal registered by the detector was maximal. When plasma appears in the grating channels in a high-voltage breakdown, the intensity of the mirror beam decreases, as shown in Fig. 27, curve *1*. As seen in Fig. 26, the characteristic time of grating switching is of the order of 5 ns.

In order to check operation of the compressor, the absorber was removed from the resonator. When the resonator was tuned to the desired resonance frequency, the signal passing through the compressor (in the mirror beam) is close to zero. When plasma develops in the grating channels, the stored energy is switched out from the resonator in a diffraction beam and, as a result, a compressed pulse is formed, also seen in Fig. 26, curve *2*. In these experiments, the half-height duration of the compressed pulse was 6-10 ns, and the power gain reached $G \approx 7$. The value of G depended on plasma homogeneity in different channels of the diffraction grating, which in turn depended on the gas pressure and simultaneity of breakdowns in all the channels of the diffraction grating.

Efficiency of energy output from the resonator, defined as the ratio of the energy in the compressed pulse to energy stored in the resonator, was measured to be in the range 40%-50%. Evidently, this relatively low value of energy output efficiency (instead of 80%-90% as theoretically possible) is a result of the fact that the time of grating switching is comparable with and even longer than the time of the passage of the electromagnetic wave through the ring resonator. During this time the gas discharge is still propagated in the grating channels, there is no output of the energy from the resonator in the necessary direction, and a part of the energy stored is scattered on the grating and lost. This effect can be mitigated significantly by making the round-trip length of the resonator greater.

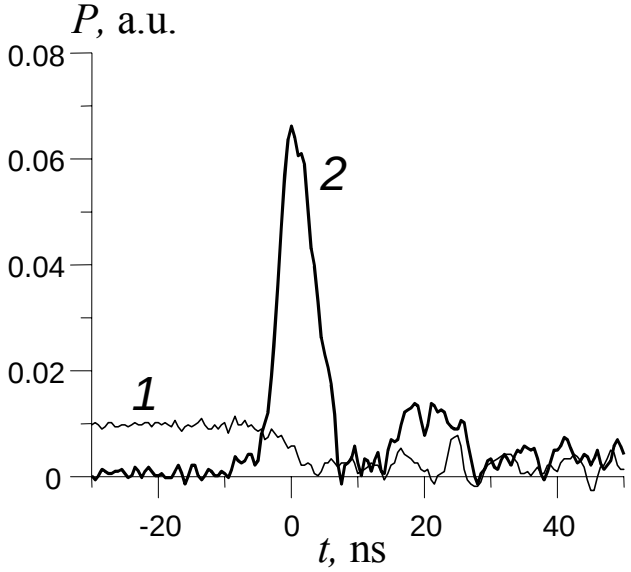

Fig. 26. Oscillograms of output signals of the active compressor when plasma is produced in the channels of the diffraction grating. *1* – signal in the mirror beam in the presence of an absorber in the resonator; *2* – compressed pulse during energy output from the resonator.

Thus, the experiments performed with the use of the non-vacuum prototype of the quasi-optical three-mirror active compressor demonstrated the feasibility of obtaining compressed pulses using an electrically controlled diffraction grating as an active element. Measured parameters of the active compressor are listed in Table 6. The preliminary experiments pointed to improvements to be taken for improving performance, including use of quartz as the material for the grating (to reduce Ohmic losses and increase unloaded resonator Q), and increasing the dimensions of the resonator (to increase output pulse width as compared with plasma discharge switching time). Nevertheless, the experiments validated the concept of the active diffraction grating as the control element in a quasi-optical millimeter-wave pulse compressor.

Table 6. Parameters of the quasi-optical three-mirror active compressor.

unloaded Q-factor	28,000
loaded Q-factor	14,000
dimensions of the diffraction grating	26×11 cm^2
material of the grating	polystyrene
power gain	~7
duration of the output pulse	6-10 ns

IIIh. Expected parameters of the quasi-optical passive and active pulse compressors

As seen from the results described in Secs. IIIb – IIIb, the concepts of passive and active quasi-optical millimeter-wave pulse compressors have been shown to have basic validity. Technical improvements should be made on prototypes to be built for high-power application, since such designs must place the entire quasi-optical circuit in a high-vacuum environment to avoid rf breakdown. This in itself will embody engineering details that might influence electrodynamic performance, so that a coordinated design is required. Here, preliminary results obtained on steps in this direction are described.

A high-power prototype of the four-mirror passive compressor, which is relatively compact, can be placed totally within a small vacuum chamber. Fig. 27 shows the top (*a*) and side (*b*) view of the design of such a vacuum chamber that encloses a four-mirror resonator. This is a design in which the all-metal diffraction grating can be easily replaced with a low-loss high-power active diffraction grating to be demonstrated as well. In this case the passive compressor becomes active. The vacuum chamber is equipped with a high-voltage feed-in for pulses to create plasma in the channels of the active diffraction grating. The completed vacuum chamber can be seen in the third photograph of Fig. 1.

The results of the studies described above show that a carefully-engineered quasi-optical four-mirror passive compressor can indeed be built that can be expected to exhibit the parameters listed in Table 7.

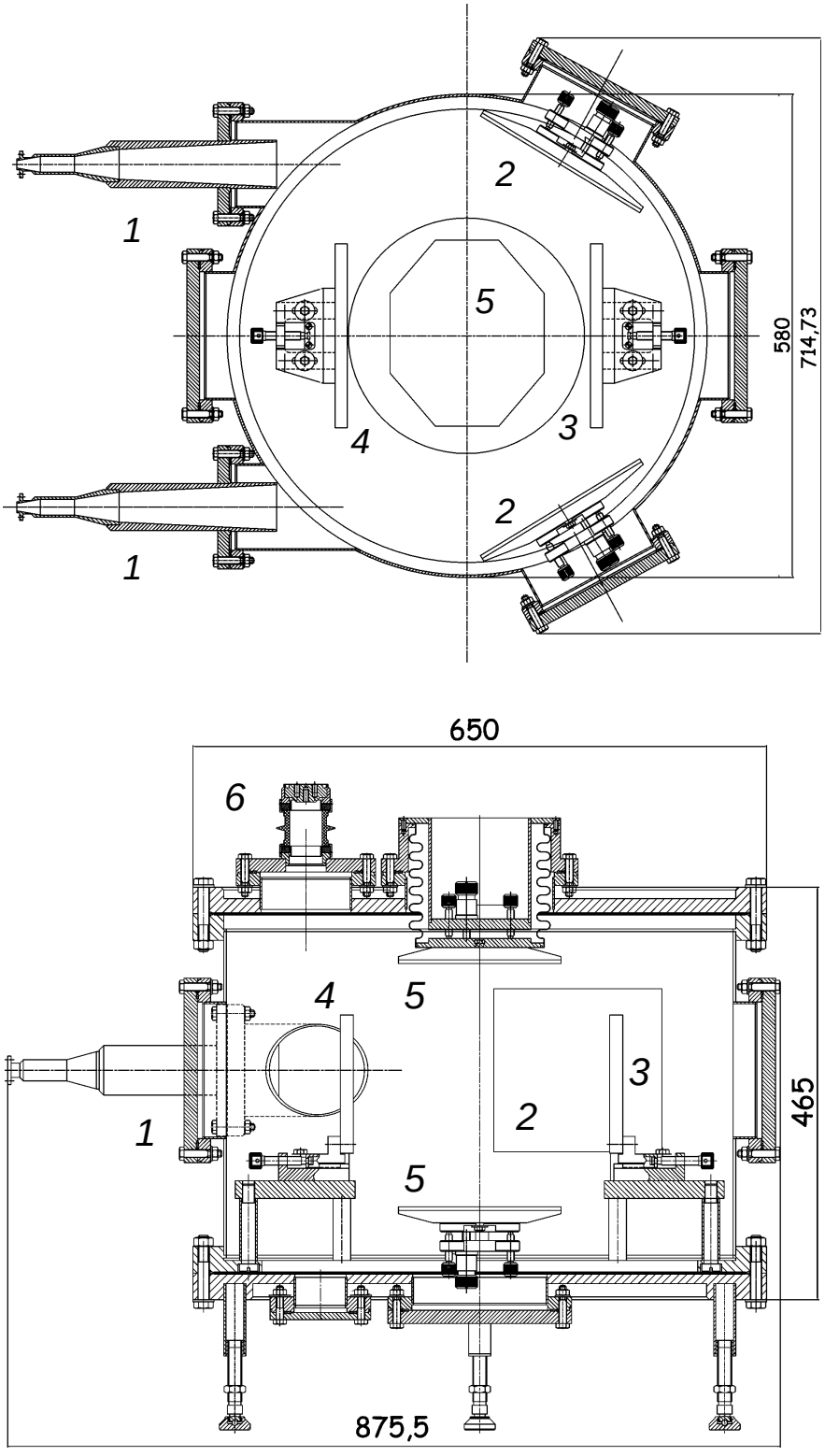

Fig. 27. Engineering design of vacuum prototype of quasi-optical passive compressor with four-mirror resonator: *1* – horn, *2* – feeding mirror, *3* – plane mirror, *4* – corrugated mirror, *5* – focusing mirror, *6* – high-voltage feed-through. See the third photograph in Fig. 1 that shows the vacuum tank as built and ready for the high-power experiments.

Table 7. Parameters of passive quasi-optical rf pulse compressor.

operating frequency	34.272 GHz
input and output modes	TE_{10}
inherent *Q*-factor	70,000
coupling *Q*-factor	4,000
duration of the input pulse	100 ns
duration of the output pulse	25 ns
compression ratio	4
efficiency, for the case of a rectangular envelope for the input pulse with linear frequency modulation	66 %
peak output power	40 MW

The four-mirror resonator with an active diffraction grating in place of an all-metal diffraction grating can be used to test active switches at high power. As seen from the previous section, developed active diffraction gratings show good promise for creation of electrically controlled wave beam switches. As described, we developed a design of an active grating made of a polystyrene, as the basis for an active switch using quartz and further test it at a high power level in the set-up shown in Fig. 27 as soon as high-power RF conditioning of one of the magnicon output transmission lines is completed, probably in Summer 2007.

The studies performed have demonstrated that operation of the quasi-optical active compressor is determined by simultaneity of gas breakdowns and homogeneity of the plasma produced in the channels of the diffraction grating. Conditions of operation of such a plasma switch will be influenced noticeably by the strong field of the wave of the ring resonator. Stability of operation of the switch can be improved by ionizing the gas in the grating channels additionally with the strongest wave of the storing resonator. This additional ionization is to e initiated by high-voltage breakdown at the moment of grating switching. Taking the effect of the microwave field into account one can expect high efficiency of energy output from the resonator and higher power gains at the levels or higher than those achieved during the preliminary tests.

Estimates show that the four-mirror compressor with such an active grating is capable of operating at high pulse powers (100–200 MW) and can have parameters listed in Table 8.

Table 8. Parameters of active quasi-optical rf pulse compressor.

operating frequency	34.272 GHz
input and output modes	TE_{10}
unloaded *Q*-factor	70000
loaded *Q*-factor (power feed/output)	40,000 / 3,000
duration of input pulse	600 ns
duration of output pulse	20-30 ns
power gain	10 – 15
output power	100 - 200 MW
efficiency	50%

Final design of a 100-200 MW high-power active compressor at 34.272 GHz will depend on results obtained during testing the electrically controlled diffraction grating at a high power level (~10 MW and over). This is clearly a key issue for future work.

IIIi. Four-mirror resonator as the basic element for a quasi-optical SLED-II

In this section we would like to point out some of merits of the four-mirror compressor design described above. When used as a passive compressor, it makes it possible to obtain a power gain of 3:1 with compression efficiency of 66% for linear frequency modulation. Based on the four-mirror resonator, it is also possible to build a two-resonator compressor, as depicted in Fig. 17, and increase the power gain and compression efficiency while retaining the same compression ratio.

Another way to improve compression efficiency and to create a near-flat-top output pulse is to transform the compressor into a quasi-optical SLED-II system using delay lines in place of the resonators. A quasi-optical mirror delay line may be made up by a series set of elementary cells, each of which is a simplified four-mirror resonator without the top and bottom mirrors. Below two samples of a quasi-optical SLED-II compressor with a mirror delay line are given. Calculations show that such compressors provide output rectangular pulses 20-27 ns long and are small and compact as well. The first example with a mirror delay line is shown in Fig. 28. The number of elementary sections is six. Its eigenmode is an axially symmetric Gaussian beam with an intensity e^{-1}-width equal to 22 mm. The distance between two adjacent mirrors measured along the beam trajectory is 520 mm. The system is 1790 mm high. The largest diameter of the system is 426 mm. The total time of radiation delay in the line, which is equal to the duration of the output pulse, is 20.8 ns. Of course, the pulse length would be larger if the number of sections were to be increased.

In order to provide a low level of diffraction losses, the dimensions of the top and bottom mirrors should be at least 200 × 115 mm, and those of the side mirrors, at least 174 × 143 mm. Mirror curvatures are $R_{\|}$ = 885 mm and $R_{\perp}$ = 594 mm. The axis of the wave beam in the delay line is directed at 55° to the normal. The delay line is excited similarly to the four-mirror resonator, as shown in Fig. 13.

A second compressor concept with a mirror delay line is shown in Fig. 29. The mirrors are situated more compactly, to make it possible to lengthen the delay and, consequently, the output pulse width. In this version of the compressor the wave beam passes from the corrugated mirror at the bottom to the top of the line twice. The full height of the compressor is 1600 mm, and its width is 442 mm. The distance between the mirrors is 624 mm and the intensity level e^{-1}-width of the Gaussian beam between the mirrors is 22 mm. The output pulse will be 73 ns long.

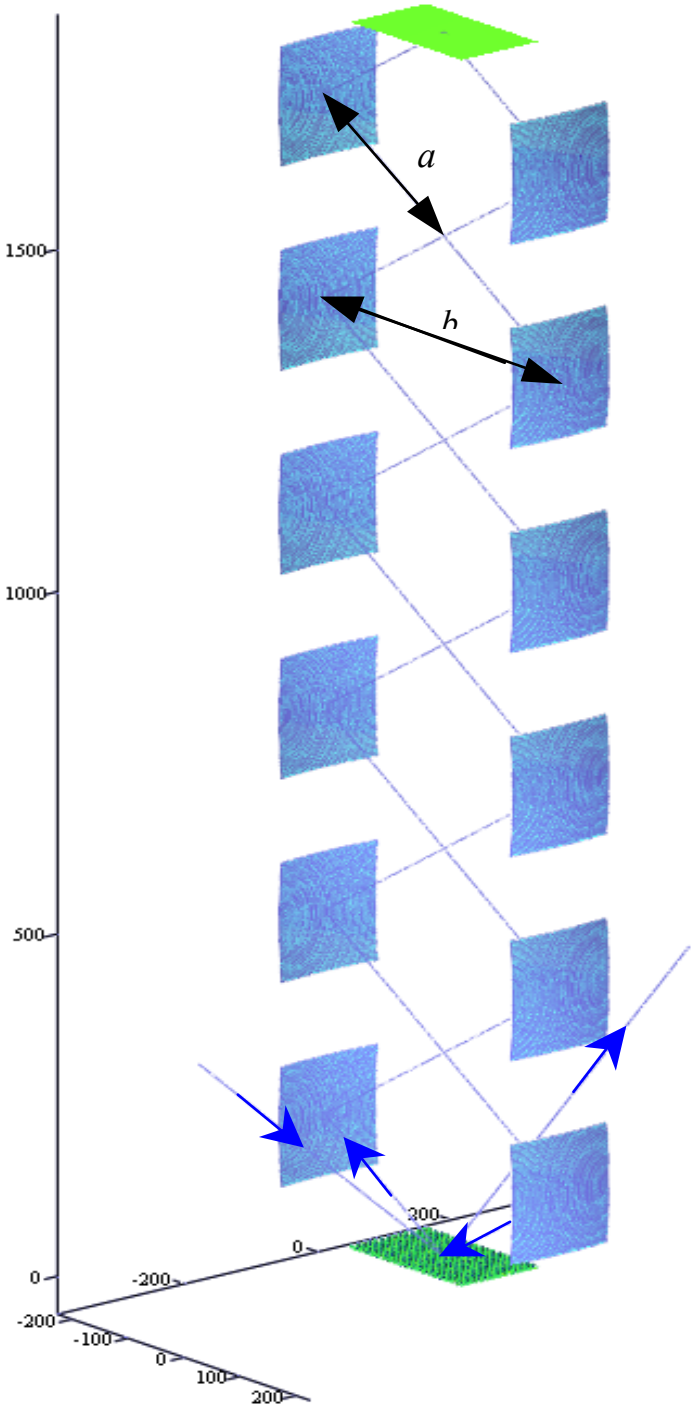

Fig. 28. Quasi-optical pulse compressor based on a multi-mirror delay line.

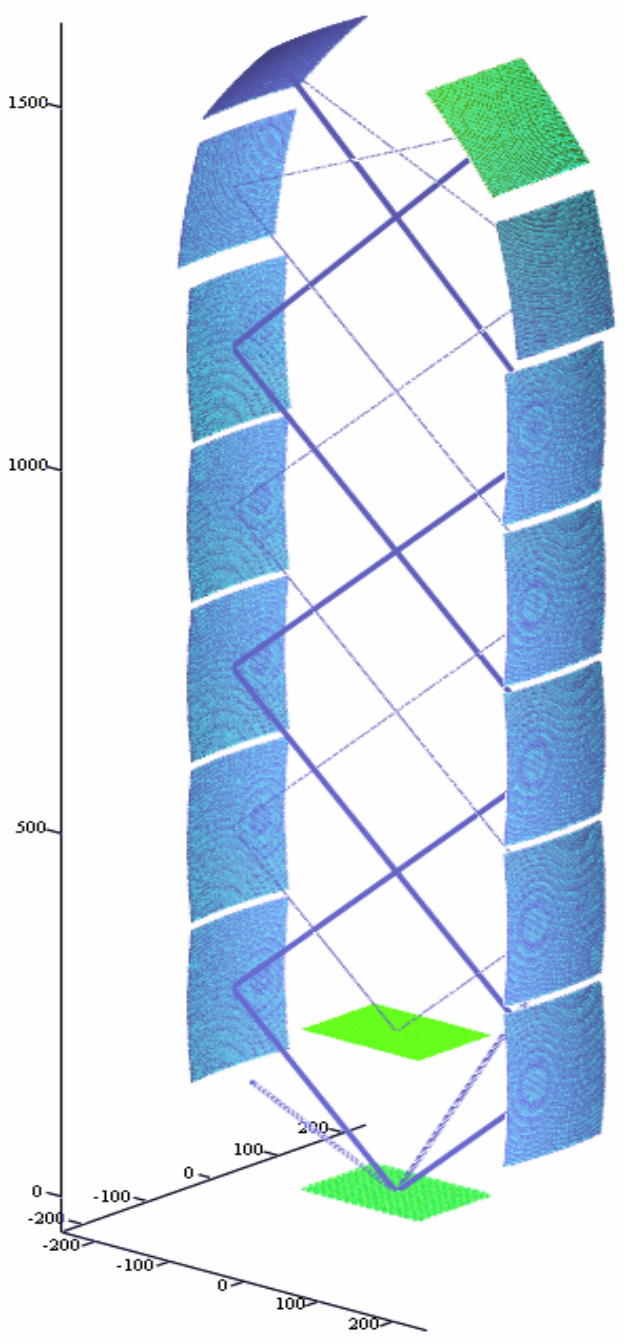

Fig. 29. Quasi-optical pulse compressor with compact mirror positioning.

IIIj. Active quasi-optical SLED-II system

The active diffraction grating described above provides the possibility of using it not only in the active four-mirror compressor, but also in compressors with mirror delay lines described in the Section IIIi. The active diffraction grating can be used to create an active quasi-optical SLED-II system operating in the 34.272 GHz frequency band.

S. G. Tantawi, R. D. Ruth and A. E. Vlieks. developed the concept of an active SLED-II system at 11.4 GHz [8]. They proposed to shift the system from the regime of energy storage to that of power output by changing both the phase of the microwave source and the coupling coefficient of the delay line. In the existing SLED-II system the resonant delay line is coupled with the input feed via an iris with a constant reflection coefficient. Replacement of the iris with an active component makes it possible to create an active SLED-II system. For an ideal actively-switched input coupler, the reflection coefficient from the active component should change from $R_0 = 0.8 - 0.96$ to $R_d = 0.4 - 0.2$ [8]. This makes it possible to achieve the following parameters of the rf pulse-compression system at 11.4 GHz band: compression ratio C = 8-16, power gain M = 7-12, and efficiency η = 70-82% depending on conductivity losses in the delay line. The same concept can be realized at 34 GHz using a mirror delay line, such as shown in Fig. 28 with an active diffraction grating as shown in Fig. 19.

These ideas are given here, not because a quasi-optical delay line is to be built as part of this project but to show that successful results obtained with passive and active quasi-optical pulse compressors using four-mirror resonators can be extended in future to systems with higher efficiency, higher output power, modular design to allow variation in output pulse width, and near-flat-top output pulses.

IV. COLD TESTS OF HIGH-POWER PROTOTYPES OF QUASI-OPTICAL Ka-BAND PULSE COMPRESSORS

In Section III, details were given to demonstrate the principal operation of the four-mirror resonator with a diffraction grating at 34 GHz and showed the potential of using this type of resonator in the future, as compared with the three-mirror resonator. The four-mirror resonator could be the basis for both a passive quasi-optical compressor and for a setup to test electrically controlled diffraction gratings required for creation of active quasi-optical compressor. In the near future, such experiments can be performed using power from the Omega-P 34.272 GHz magnicon.

Therefore, the overall objectives for cold tests to be described here are to optimize parameters of the four-mirror resonator with linear frequency modulation in the input magnicon pulse; to manufacture the vacuum four-mirror passive compressor; and to test this compressor connected to one channel of the magnicon in order to obtain ~40 MW compressed pulses and then to test the electrically controlled diffraction grating made of quartz placing it instead of metal diffraction grating of the resonator. All but the last—albeit most important—of these tasks have been accomplished, as reported here. The specific work included the following. Further theoretical study was carried out for the four-mirror resonator in order to optimize the parameters of the passive compressor for operation with the magnicon Design, fabrication and low-power test of non-vacuum prototype of the four-mirror passive compressor with linear frequency modulation in the input pulse generated by the klystron generator were carried out. Design and fabrication of the vacuum version of the four-mirror passive compressor was completed. Cold-test measurements of the vacuum version of the four-mirror passive compressor were carried out. Fabrication of the electrically controlled (active) diffraction grating was carried out. Further theoretical (numerical) study of active diffraction gratings was carried out. Design, fabrication and low-power tests of the non-vacuum active switch made of polystyrene was carried out. Design and fabrication of the vacuum version of the active switch made of quartz was carried out.

IVa. Low power tests of quasi-optical three and four mirrors resonators

We have performed low-power tests of four- and three-mirror quasi-optical resonators to be used as passive compressors of microwave pulses. In the experiment the resonator mirrors were placed in the vacuum chamber, and the resonator was tuned from the outside by means of adjustment devices. The experiment was performed under atmospheric pressure in the chamber. Fig. 27 shows an engineering drawing of the vacuum chamber designed to accommodate either the three- or four-mirror resonator, and the latter with either a passive or active grating. A photo of the vacuum chamber is seen in the third part of Fig. 1. Parameters of four-mirror quasi-optical passive compressor are describe in the following paragraph.

A four-mirror compressor of microwave pulses is a high-Q-factor quasi-optical travelling-wave resonator formed by copper mirrors, a corrugated (4) and a plane (3) mirror, and two parabolic mirrors (5). The scheme of high-vacuum four-mirror quasi-optical resonators with an excitation system is shown in Fig. 30, which depicts the mirror system as installed in the vacuum chamber. A photograph is shown in Fig. 31.

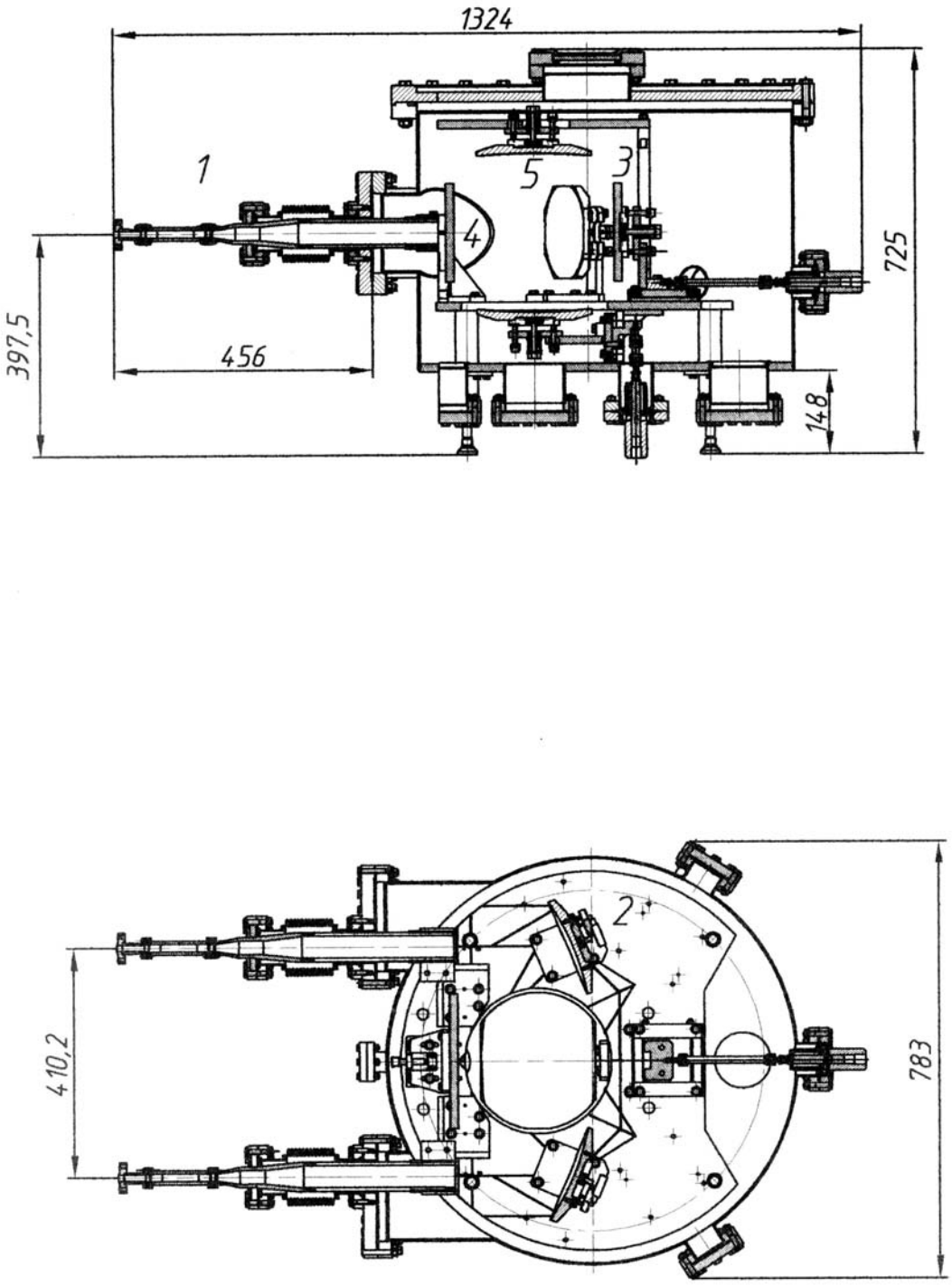

Fig. 30. Drawing of the high-vacuum 34 GHz quasi-optical four-mirror resonator: *1* — horn, *2* — adjustment mirror, *3* — plane mirror, *4* — corrugated mirror, *5* — focusing mirror.

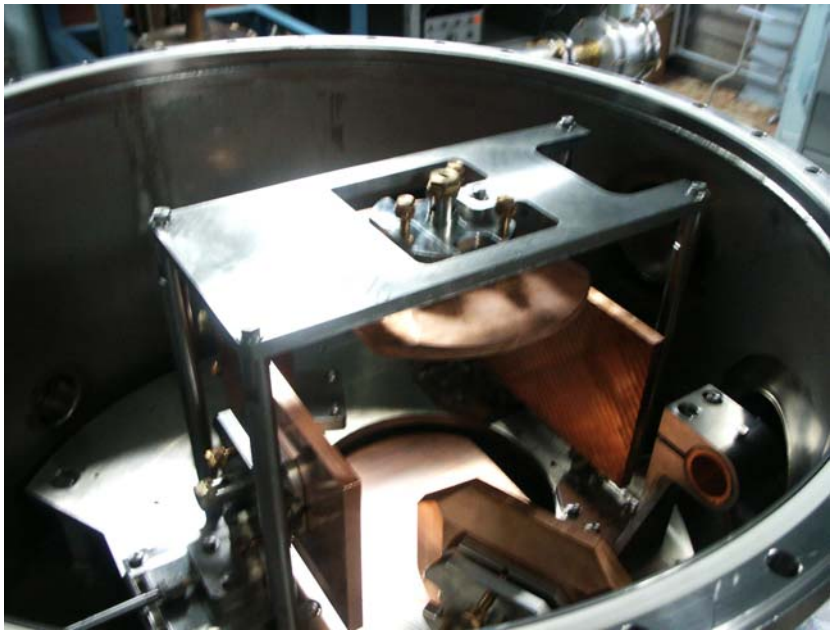

Fig. 31. Disposition of the mirrors of the four-mirror resonator in the vacuum chamber.

The four-mirror resonator is excited in the TE_{00n} mode through a waveguide excitation system (input channel), which consists of a tapering horn (*1*), a polarizer, and an adjustment mirror (*2*). A similar system is used to output the energy from the resonator (output channel). All the mirrors of the resonator are equipped with adjustment devices, which make it possible to displace the mirrors using the adjusters outside the chamber. Thus, the resonator frequency can be tuned without disrupting the vacuum in the chamber.

Radiation of the diagnostic microwave generator enters the input channel of the resonator in the TE_{01} mode of a rectangular waveguide and is transformed into a wave beam with a Gaussian distribution over the transverse coordinate by means of the input horn (*1*). This radiation is sent to the corrugated mirror (*4*), which is a diffraction grating, by means of the adjustment mirror (*2*). In this case the required orientation of the electric field vector relative to the diffraction grating is set by means of a polarizer installed in front of the input horn. The main share of the power is reflected mirror-wise from the surface of the corrugated mirror into the output channel of the compressor. Thus, there is no wave reflected back into the generator (input channel) and, hence, it does not impact on the operation of the microwave generator. The output channel of the resonator is absolutely identical to the input channel, and consists of the adjustment mirror, the horn, and the polarizer as well. The radiation fed to the input of the channel as a Gaussian beam is converted into the TE_{01} mode of rectangular waveguide at its output.

At first, we measured the coefficient of power transmission from horn to horn along the waveguide-mirror line. The diffraction grating in this case was replaced with a plane mirror. The transmission coefficient, $K = P/P_0$, was determined as the ratio of the power in the output channel P, to the power fed to the input horn P_0. The measured values of K ranged from 92% to 93%, depending on the mirror adjustment, which is somewhat lower than the calculated value of 98%.

When the corrugated mirror was installed, a part of the microwave power (~6%) is branched into the first diffraction maximum of the corrugated mirror and used to excite the four-mirror resonator. The travelling-wave regime settles in the resonator. The wave that propagates through the resonator is also scattered on the corrugated mirror, and a part of its power enters the output channel of the compressor. In the output channel, the mirror-reflected wave and the wave leaving the resonator are added in phase opposition. Therefore, when the frequency of the microwave pulse coincides with the resonator frequency, the amplitude of the signal in the output channel drops sharply. Then, the Q-factor of the resonator was measured. The measurements were performed by two methods: from the half-width of the resonant curve using a spectrum analyzer, and from decay of the trailing edge of the radiation leaking from the resonator after the end of the microwave pulse. Fig. 32 shows an oscillogram of the incident power P_0, and the transmitted power P, when the resonator was excited with a long rectangular pulse.

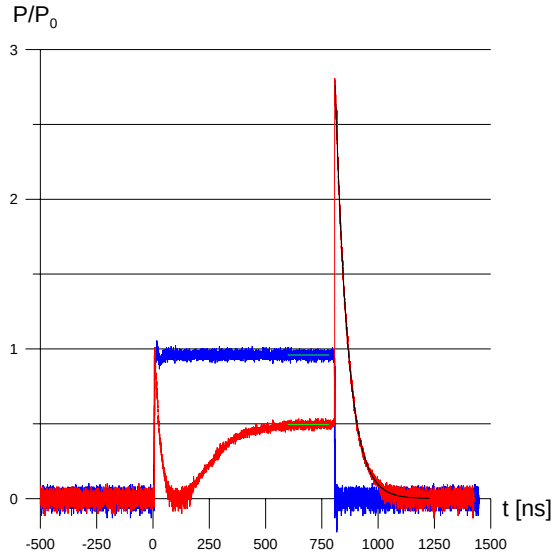

Fig. 32. Red curve is the output pulse of power P. Blue curve is the input pulse of power P_0. Black curve is the exponent that approximates damping at the trailing edge. Green curves are asymptotes for stationary transmission coefficients out of resonance and in resonance.

The drop of the power at the trailing edge of the pulse is determined by the expression

$$P(t) = P_{max} \cdot \exp(-t/\tau) , \qquad (9)$$

where $\tau = Q_L/\omega$, and Q_L is the loaded Q-factor. The loaded Q-factor of the resonator obtained from the trailing edge of the pulse equalled Q_L =12,200, and agreed well with the Q-factor determined from spectral measurements, i.e., Q_L =12,700. In turn, the loaded Q-factor is connected with the coupling Q-factor, Q_e, and inherent Q-factor, Q_0, via the expression

$$1/Q_L = 1/Q_e + 1/Q_0. \qquad (10)$$

The coupling Q-factor and the inherent Q-factor of the resonator were determined for a long microwave pulse from the ratio of stationary transmission coefficients out of resonance P_{in} and in resonance P_{out}, in accordance with the formula

$$P_{out}/P_{in} = \left(\frac{1-\beta}{1+\beta}\right)^2 , \qquad (11)$$

where $\beta = Q_0/Q_e$. The values of the Q-factors determined by using Eqs. (9), (10), and (11) are shown in Table 9.

Table 9. Quality factors for the four-mirror cavity.

Measurement method	Q_L	Q_e	Q_0
Spectrum analyzer	12,700	14,300	11,3000
Long pulse	12,200	14,300	82,300
Calculation	12,250	12,650	500,000

It is seen from the table that the measurement results are in good agreement with the calculated results. Some deviations in values of the inherent Q-factor (determined by Ohmic and diffraction losses in the resonator) are associated with imprecise data about Ohmic losses on the mirrors used in calculation. Note that the parameters of the four-mirror resonator were optimized for the expected parameters of the magnicon pulse: pulse duration of 250 ns, and a frequency variation along the pulse of 15 MHz.

IVb. Tests of high-vacuum passive compressor with a four mirror resonator

In a set of the experiments we tested the compressor with linear frequency modulation. In the case of the linear frequency modulation the compressor was tested in the setup shown in Fig. 33. The tests were performed for the pulse parameters corresponding to the following parameters of the magnicon pulse: resonance frequency $f_0 = 34.273$ GHz, duration of the input pulse $\tau = 257$ ns, variation of the frequency along the pulse, $\Delta f_g = 14.7$ MHz.

A block diagram of the experimental setup included several generators: the Gunn-diode microwave generator with a built-in varicap (*1*), the generator of pulses with controlled shapes to control the frequency of the microwave generator by sending a voltage pulse to the varicap (*2*), the electrically controlled former of the envelope of microwave pulses (*3*), and the generator feeding the envelope former (*4*). The required rate of frequency tuning to create the necessary linear frequency modulation was achieved by setting the corresponding rate of voltage build-up in the controlling pulse of generator (*2*). In this case, separate calibration of the dependence of the frequency of the microwave generator (*1*) on the voltage applied was taken into account. A sample of the oscillograms of the input pulse are shown in Fig. 34. The optimal initial frequency detuning from the resonant frequency was sought directly during the experiment by means of varying the constant component of the pulse amplitude in generator (*2*).

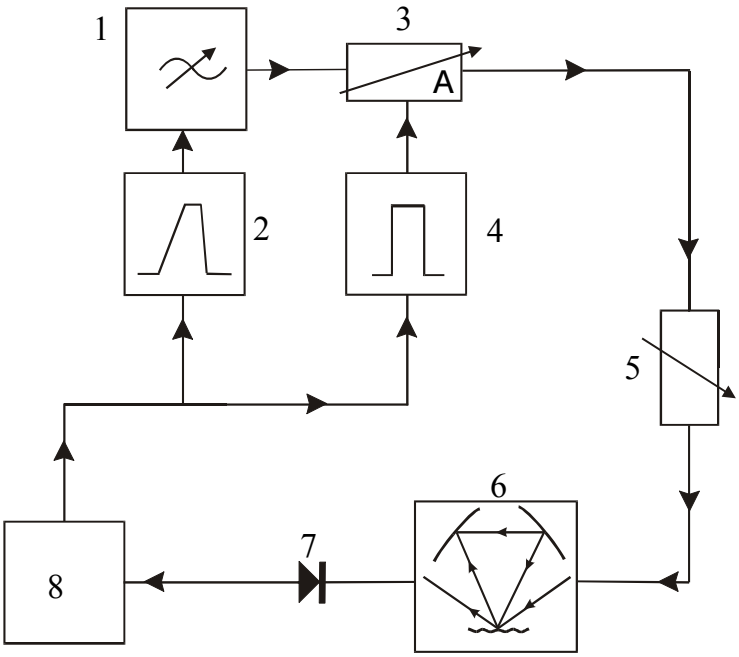

Fig. 33. The scheme of the experimental setup in the case of the linear frequency modulation. 1 - microwave generator, 2 – generator of pulses; 3 – former of envelope, 4 - pulse generator, 5 - high-precision attenuator; 6 - analyzed resonator; 7 - detector; 8 - oscilloscope.

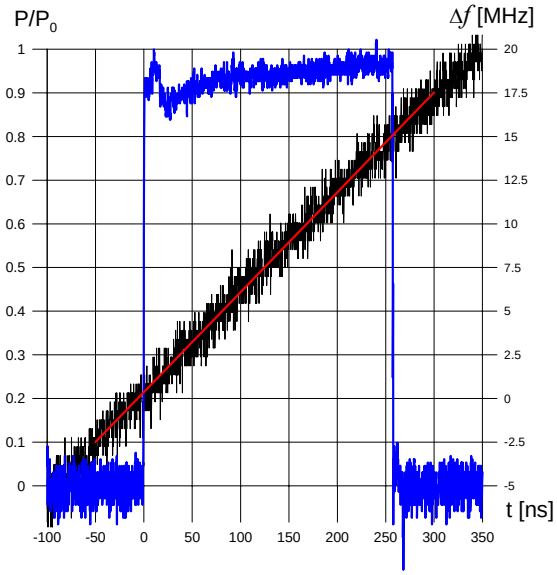

Fig. 34. Formation of a rectangular pulse with a preset linear frequency modulation (LFM). Blue curve is the input LFM pulse. Black curve is the time dependence of the generator frequency. Red curve is the linear function that approximates the frequency time dependence.

Samples of the oscillograms of the output pulses obtained using this method of compressor operation and results of calculations are shown in Fig. 35.

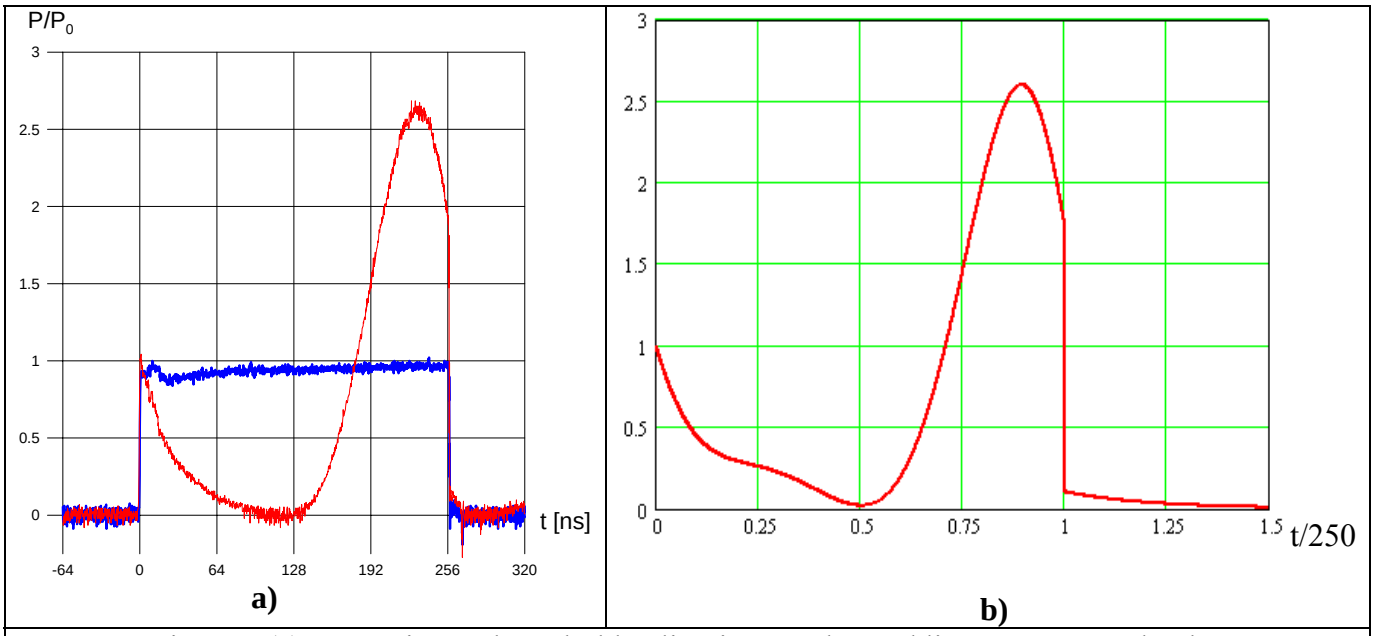

Fig. 35. (a) – experimental result: blue line-input pulse, red line –compressed pulse
(b) – results of calculation

Experimental characteristics of compressed pulses and parameters of compressor operation are listed in Table 10.

Table 10. Compression of experiment and theory with linear frequency modulation.

	Pulse duration τ, ns	Frequency modulation Δf_g, MHz	Compression ratio, S	Efficiency η, %	Power gain P_g
Experiment	257	14.7	4	57	2.6
Theory	250	15	4	55.6	2.6

IVc. Parameters of three-mirror quasi-optical resonator

The three-mirror resonator is planned to be used in the quasi-optical microwave compressor with an active diffraction grating. A photo of the disposition of mirrors in the vacuum chamber for the three-mirror resonator is shown in Fig. 36.

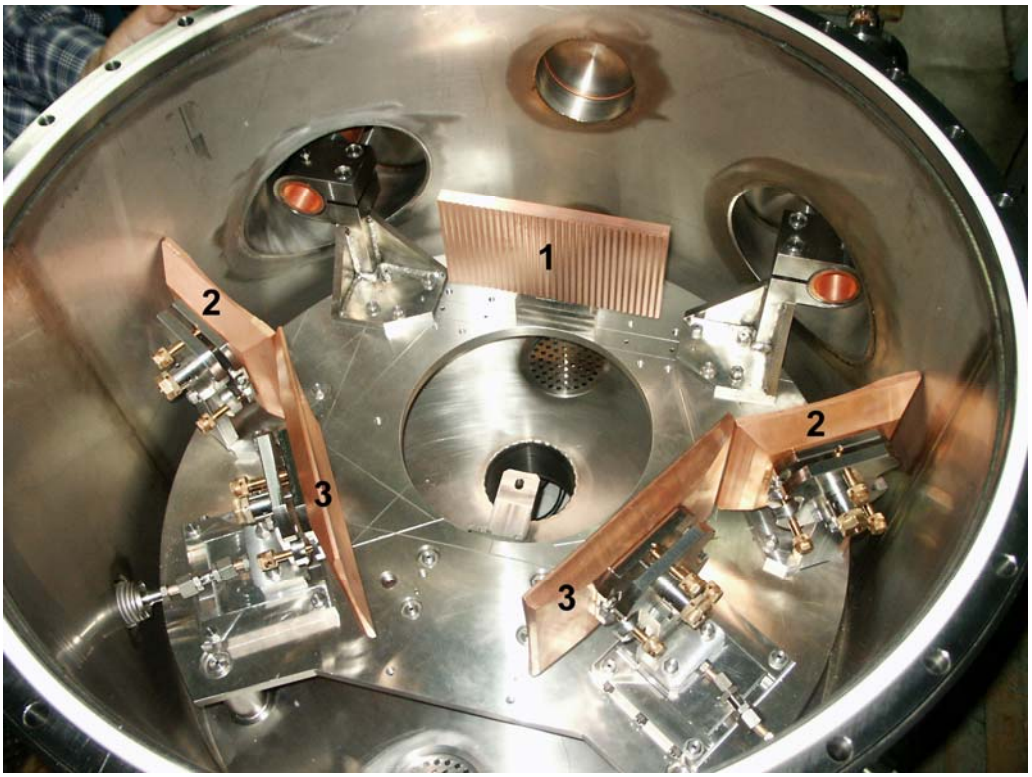

Fig. 36. Photo of the three-mirrors resonator installed in the vacuum chamber in place of the four-mirror resonator: *1* — corrugated mirror (diffraction grating), *2* — adjustment mirror, *3* — parabolic focusing mirror.

Currently the active quartz grating is being manufactured, so that initial tests have been performed with a metal diffraction grating. The measurements of the *Q*-factor were performed by the same method as in the four-mirror resonator. The results of the measurements are shown in Table 11.

Table 11. Quality factors for the three-mirror cavity.

	Q_L	Q_e	Q_0	K
experiment	12,700	13,700	160,000	94 %
calculation	12,600	12,930	500,000	98 %

Thus, the experiments that were carried out demonstrated good qualitative and quantitative correlation of theory and experiment both for the four- and three-mirror resonators.

Photographs of the prototype active grating, with and without discharges in the grating grooves, are shown in Fig. 37.

Fig. 37. Photographs of the prototype active grating.

V. CONCLUSIONS

Designs have been carried out on non-high-vacuum, low-power versions of three- and four-mirror quasi-optical passive and active Ka-band pulse compressors, and prototypes built and tested based on these designs. The active element is a quasi-optical grating employing gas discharge tubes in the gratings. Power gains of about 3:1 were observed experimentally for the passive designs, and about 7:1 with the active designs. High-power, high-vacuum versions of the three-and four-mirror quasi-optical pulse compressors were built and tested at low power. These now await installation and testing using multi-MW power from the 34-GHz magnicon.

References

1. Nezhevenko O.A. et al., "High power pulsed magnicon at 34 GHz," RF98 Workshop, Pajaro Dunes, CA, October 5-9, 1998.

2. Nezhevenko O.A. et al., "Commissioning of the 34 gHz, 45 MW pulsed magnicon," *IEEE Trans. On Plasma Science* **32**, no. 3, June 2004, pp. 994-1001.

3. Denisov G.G., Kuzikov S.V., Bogdashev A.A., Chirkov A.V., Hirshfield J.L., Litvak A.G., Malygin V.I., Shmelyov M.Yu., Study of Ka-band components for future high-gradient accelerators, Advanced Accelerator Concepts, 10th Workshop, C.E.Clayton and P.Muggli, eds, AIP Conf. Proc., 2002, v.647, pp.476-483.

4. Vikharev A.L., Danilov Yu.Yu., Gorbachev A.M., Kuzikov S.V., Koshurinov Yu.I., Paveliev V.G., Petelin M.I., Hirshfield J.L., Quasi-optical microwave pulse compressor at 34 GHz, Advanced Accelerator Concepts, 10th Workshop, C.E.Clayton and P.Muggli, eds, AIP Conf. Proc., 2002, v.647, pp.448-458.

5. Petelin M.I., Quasi-optical collider concept, Advanced Accelerator Concepts, 10th Workshop, C.E.Clayton and P.Muggli, eds, AIP Conf. Proc., 2002, v.647, pp.459-468.

6. Wilson P.B., "Scaling linear colliders to 5 TeV and above," SLAC-PUB-7449, April, 1997.

7. Tantawi S.G. et al., "High-power multimode X-band RF pulse compression system for future linear colliders," PRST-AB **8**, 042002 (2005).

8. Tantawi S.G., Ruth R.D. and Vlieks A.E., Active radio frequency pulse compression using switched resonant delay lines, Nuclear Instruments and Methods in Physics Research A, 1996, v.370, pp.297-302.

9. Fox A.G., Li T., Bell System Techn. J., 1961, Vol. 40, No. 2, pp. 453-464.

10. Petelin M.I, Hirshfield J.L., Kuzikov S.V., Vikharev A.L., "High power microwave pulse compressors: passive, active, and combined," Proc.of SPIE's 14th Annual Symposium on Aerosense, 24-28 April 2000, Orlando, Florida USA.

11. Petelin M.I., Tai M.I., "Compression of phase-modulated microwave pulse by chain of ring cavities," Proc. of AIP Conf. 337, Pulsed RF sources for linear collider, Montauk, NY, 1994, pp.303-310.

12. Yee K.S., IEEE Trans. Antennas and Propagation, v. AP-14, 302 (1966).